

University of Nebraska - Lincoln

DigitalCommons@University of Nebraska - Lincoln

Department of Mechanical and Materials
Engineering: Dissertations, Theses, and Student
Research

Mechanical & Materials Engineering,
Department of

12-2023

An ICFD Fluid Model Used in a MASH TL-6 Vehicle Model

Md Zunayed Habib

University of Nebraska-Lincoln, zhabib2@huskers.unl.edu

Follow this and additional works at: <https://digitalcommons.unl.edu/mechengdiss>



Part of the [Materials Science and Engineering Commons](#), and the [Mechanical Engineering Commons](#)

Habib, Md Zunayed, "An ICFD Fluid Model Used in a MASH TL-6 Vehicle Model" (2023). *Department of Mechanical and Materials Engineering: Dissertations, Theses, and Student Research*. 190.
<https://digitalcommons.unl.edu/mechengdiss/190>

This Article is brought to you for free and open access by the Mechanical & Materials Engineering, Department of at DigitalCommons@University of Nebraska - Lincoln. It has been accepted for inclusion in Department of Mechanical and Materials Engineering: Dissertations, Theses, and Student Research by an authorized administrator of DigitalCommons@University of Nebraska - Lincoln.

**AN ICFD FLUID MODEL USED IN A MASH TL-6 VEHICLE
MODEL**

by

Md Zunayed Habib

A THESIS

Presented to the Faculty of
The Graduate College at the University of Nebraska
In Partial Fulfillment of Requirements
For the Degree of Master of Science

Major: Mechanical Engineering and Applied Mechanics

Under the Supervision of Professor Cody Stolle

Lincoln, Nebraska

December 2023

AN ICFD FLUID MODEL USED IN A MASH TL-6 VEHICLE MODEL

Md Zunayed Habib, M.S.

University of Nebraska, 2023

Advisor: Cody Stolle

The objective of this thesis was to develop an ICFD finite element model of a partially filled deformable container suitable for impact scenarios. This model will be later incorporated into the existing TL-6 vehicle model, which is a tractor-tank trailer vehicle model. Previous finite element fluid models for the TL-6 vehicle used an elastic fluid model, which could not predict the fluid behavior correctly.

A study was conducted on the ICFD modeling and an improved ICFD model has been developed using the LS-DYNA, a finite element analysis software. Different properties and parameters of the fluid and the container were adopted from the previous models and scientific research publications.

The ICFD model was a cylindrical capsule of 2 m long and 1 m wide, containing a ballast of 284 gallons of water. Impact condition of 20 m/s speed to a rigid wall was simulated. The model was able to achieve the fluid sloshing behavior ensuring no leakage of fluids from the model. There was no warpage or shooting of elements, the model was stable and robust. Therefore, it was considered an improvement to the previous elastic models used in the TL-6 vehicle model.

ACKNOWLEDGEMENTS

First and foremost, I express my gratitude to my creator and Lord, Allah, for the invaluable gift of life and prosperity. I extend my sincere appreciation to my advisor, Dr. Cody Stolle, whose experience, guidance, and unyielding support have been instrumental in shaping me into a better researcher and individual. I am truly thankful for your keen interest in my personal, educational, and professional development, and for the wisdom and direction you have generously provided.

I also wish to acknowledge the Midwest Roadside Safety Facility (MwRSF) and my esteemed colleagues during my tenure there. The research opportunity, resources, and support provided by the MwRSF have been pivotal to the success of this endeavor.

Special recognition is extended to Livermore Software Technology Corporation (LSTC) for their provision of LS-DYNA. I am grateful for the computing resources at the Holland Computing Center (HCC) at the University of Nebraska-Lincoln, which played a crucial role in the execution of this research.

My heartfelt thanks go to my parents for their unwavering belief in me. Their inspiration and support have enabled me to pursue education at a distinguished university despite the geographical distance of 9000 miles from home.

I convey profound gratitude to my closest friend and loving wife, Mala, for her enduring love, unwavering support, and constant inspiration. Her presence by my side during both the joys and challenges has been my pillar of strength. I am particularly thankful for her care during this journey, and I recognize that overcoming these difficulties would not have been possible without her steadfast support.

Finally, I dedicate this thesis to my beloved daughter, Zunyra, whose arrival brought immeasurable joy to my life. Her presence has been a source of inspiration and motivation throughout most of this academic journey.

TABLE OF CONTENTS

ACKNOWLEDGEMENTS	IV
TABLE OF CONTENTS	VI
LIST OF FIGURES	VIII
1 INTRODUCTION	1
1.1 BACKGROUND	1
1.2 RESEARCH OBJECTIVE	2
1.3 RESEARCH SCOPE.....	3
2 LITERATURE REVIEW	4
2.1 FLUID MODEL IN WHITFIELD’S AND VASQUEZ’S TL-6 VEHICLE MODEL.....	4
2.2 INCOMPRESSIBLE COMPUTATIONAL FLUID DYNAMICS (ICFD) IN LS-DYNA.....	5
2.2.1 Automatic Volume Meshing- Delaunay Criterion.....	8
2.2.2 Free surface- Level set method	9
2.2.3 FSI coupling methods in ICFD.....	11
2.2.4 Boundary Conditions	13
2.3 DISCUSSION	15
3 INITIAL FLUID DYNAMICS SIMULATION	16
3.1 2D FLUID FLOW SIMULATION OVER A CYLINDER	16
3.1.1 Mesh generation.....	16
3.1.2 Model Setup.....	17
3.1.3 Results.....	19
3.2 FLUID IN A 3D CONTAINER EXCITED PERIODICALLY	23
3.2.1 Mesh Generation and model setup.....	24
3.2.2 Results.....	26
3.3 FSI MODEL SIMULATION	30
3.3.1 Model Setup.....	30
3.3.2 Results.....	33
4 ICFD-FSI MODEL FOR A DEFORMABLE CONTAINER	37
4.1 Introduction.....	37
4.2 Model details.....	37
4.2.1 The deformable container model	37
4.2.2 The ICFD model for the container	38
4.2.2 ICFD and FSI controls and other cards.....	41
4.3 Impact Simulation Results	44
4.4 Difficulties	49
4.5 TL-6 ICFD Fluid Model Development.....	51
5 COMPARISON BETWEEN ICFD AND LAGRANGIAN MODEL.....	53

	vii
5.1 Introduction.....	53
5.2 Model description	53
5.3 Simulation Results	53
5.4 Discussion.....	62
6 SUMMARY AND CONCLUSION	63
7 FUTURE WORKS.....	65
8 REFERENCES	66
9 APPENDIX.....	68

LIST OF FIGURES

Figure 1. Whitfield’s Model (Top) and Vasquez’s Model (Bottom) [7].	4
Figure 2. Delaunay criterion. a) Satisfied b) Violation	9
Figure 3. Different types of Level set methods [8].	11
Figure 4. Two types of FSI coupling [8].	12
Figure 5. a) Non-slip Boundary condition, b) Free slip Boundary condition	14
Figure 6. Geometry, Mesh, and Parts	17
Figure 7. Part, Material, Section cards of Example 1	17
Figure 8. Mesh cards of example 1	18
Figure 9. Boundary, and Initial Conditions of Example 1	18
Figure 10. Results with velocity fringe plots of example 1	19
Figure 11. Results with velocity fringe plots of example 1(cont.)	20
Figure 12. Results with velocity fringe plots of example 1(cont.)	21
Figure 13. Mesh adaptation, Sequential image in example 1	22
Figure 14. Mesh and parts of example 2. (Sectional view on the lower image)	25
Figure 15. Sequential image of the simulation of example 2	26
Figure 16. Sequential image of the simulation of example 2	27
Figure 17. Sequential image of the simulation of example 2	27
Figure 18. Sequential image of the simulation of example 2	28
Figure 19. Sequential image of the simulation of example 2	28
Figure 20. Sequential image of the simulation of example 2	29
Figure 21. Sequential images of Fluid sloshing in Xue et.al. model [11].	29
Figure 22. Sequential images of Fluid sloshing in Xue et.al. model [11]. (cont.)	30
Figure 23. The model setup of example 3.	31
Figure 24. The model setup, hiding the sidewall, in example 3	31
Figure 25. Overlapping elements at the FSI surface.	32
Figure 26. Additional Inputs Required for FSI Example.	33
Figure 27. Fluid Velocity fringe plots around the flaps.	34
Figure 28. The displacement at the free ends of the flaps.	34
Figure 29. Deformation in the flaps due to fluid flow	35
Figure 30. Stress profiles in the flaps. (Von Mises Stress)	35
Figure 31. The pressure profile on the flaps.	36
Figure 32. Model inputs for cylindrical capsule	37
Figure 33. The deformable container model.	38
Figure 34. Surface elements of the deformable container model	39
Figure 35. Cross-sectional view of the surface elements of the deformable container	40
Figure 36. Model inputs for ICFD-capsule problem	41
Figure 37. FSI control inputs	42
Figure 38. Additional ICFD control cards used in capsule simulation.	43
Figure 39. Implicit model controls for coupled implicit-explicit model solutions.	44
Figure 40. Sequential image of the deformable container, impacting rigid wall, t=5.1 ms.	45
.....	45

Figure 41. Sequential image of the deformable container, impacting rigid wall, $t=17.6$ ms.	45
Figure 42. Sequential image of the deformable container, impacting rigid wall, $t=25.6$ ms.	45
Figure 43. Sequential image of the deformable container, impacting rigid wall, $t=49.6$ ms.	46
Figure 44. The sectional view of the level sets of the simulation, $t=5.1$ ms.	47
Figure 45. The sectional view of the level sets of the simulation, $t=17.6$ ms.	47
Figure 46. The sectional view of the level sets of the simulation, $t=25.6$ ms.	48
Figure 47. The sectional view of the level sets of the simulation, $t=49.6$ ms.	48
Figure 48. Fluid volume in the deformable container during impact simulation.	49
Figure 49. The change in velocity during impact simulation	49
Figure 50. TL-6 tanker, container models with baffles.	51
Figure 51. ICFD model simulation screenshot at impact, ($t=0$ ms).	54
Figure 52. Elastic model simulation screenshot at impact, ($t=0$ ms).	54
Figure 53. ICFD model simulation screenshot during impact ($t=10.5$ ms).	55
Figure 54. Elastic model simulation screenshot at impact, ($t=10$ ms).	55
Figure 55. ICFD model simulation screenshot after impact, ($t=20.5$ ms).	56
Figure 56. Elastic model simulation screenshot at impact, ($t=20$ ms).	56
Figure 57. ICFD model simulation screenshot after impact, ($t=32.5$ ms).	57
Figure 58. Elastic model simulation screenshot at impact, ($t=32$ ms).	57
Figure 59. ICFD model simulation screenshot after impact, ($t=44.5$ ms).	58
Figure 60. Elastic model simulation screenshot at impact, ($t=44$ ms).	58
Figure 61. ICFD model simulation screenshot after impact, ($t=58.5$ ms).	59
Figure 62. Elastic model simulation screenshot at impact, ($t=58$ ms).	59
Figure 63. Initial velocity to the structure only (Lagrangian model).	60
Figure 64. Element inversion in Lagrangian model.	61
Figure 65. Global X-velocity change of the containers.	62

1 INTRODUCTION

1.1 Background

In 2022 about 42,795 people lost their lives on the road [1]. This number has been greatly reduced when roadside safety features were introduced. There are roadside barriers, bridge rails, and median barriers to minimize damage and prevent errant motorists from striking roadside fixed objects, such as poles, trees, etc. These also prevent errant vehicles from running off the road. For instances where there could be a running off-road situation, barrier systems are installed with a view to safely containing and redirecting the vehicles. The functionality of the safety barriers is evaluated according to the Test Level 3 (TL-3) to Test Level 6 (TL-6) safety performance guidelines published in either National Cooperative Highway Research Program (NCHRP) Report No. 350, Recommended Procedures for the Safety Performance Evaluation of Highway Features [2] or the Manual for Assessing Safety Hardware (MASH) by American Association of State highway and Transportation Officials (AASHTO) [3].

On May 11, 1976, a tractor-tank trailer transporting 7,509 gal of anhydrous ammonia lost control and impacted the bridge rail on the ramp connecting Interstate 610 (I-610) to the Southwest Freeway (U.S. 59) in Houston, Texas [4]. As a result of the ammonia leak from this incident, six people were killed, 78 were hospitalized, and approximately an additional 100 people were treated for other related injuries. On January 13, 2004, a tractor-tank trailer carrying 8,800 gal of gasoline left the roadway in Elkridge, Maryland, and collided with the bridge rail of the ramp it was on, causing the tractor-tank trailer to roll over the top of the barrier [5]. The vehicle subsequently fell 30 ft onto the

roadway below at which time it exploded and caught fire. The fire from the leaked gasoline destroyed five vehicles and caused four fatalities.

A TL-6 test condition utilizes a tractor tank trailer, an 80,000-lbs. vehicle, impacting the barrier at a speed of 62 mph (100 kph) at a 15-degree angle. TL-6 barriers are installed at places where there is a higher chance of running off-road and a higher possibility of infrastructural damage. Preparation for a MASH TL-6 test is expensive and time-consuming, so before performing a test, the feasibility and the outcome of the test are predicted using finite element modeling of the test. This requires a model for the barrier and a model for the vehicle. There exists a vehicle model and there is a need for a more accurate and efficient model of the fluid inside the tank to model the TL-6 test.

LS-DYNA is a finite element analysis (FEA) program developed by Livermore Software Technology Corporation (LSTC). LS-DYNA is popular among researchers of various concentrations such as construction, manufacturing, bioengineering, materials engineering, automobile-aeronautical engineering, and many more. It allows its user to perform highly nonlinear transient dynamic analysis using explicit time integration.

1.2 Research Objective

The objective of this research effort was to develop an fluid model of the fluid inside the TL-6 vehicle model using LS-DYNA with Incompressible Computational Fluid Dynamics (ICFD) solver. The following criteria were used to judge the progress of the research objective: (1) The proposed model demonstrates improvement over the existing elastic fluid model, showing proper fluid behavior, i.e., sloshing. (2) the model must be concise and easily constructed, and (3) the model must be stable and not prone to non-

physical modeling results. In addition, the limitations and future work on the model required consideration.

1.3 Research Scope

The research objective was achieved through various steps. First, a study was performed for previously modeled TL-6 fluid models and fluid surface interactions using finite element analysis. Shortcomings of previous models were identified, and a new modeling approach was selected (ICFD). Then, different simple ICFD models were developed and validated against published simulation results. Various properties of the fluids were collected from various research articles, where fluids were modeled with ICFD. An ICFD model was implemented in a cylindrical tank identical to the TL-6 vehicle model but at a smaller scale. In This ICFD model simulation, the sloshing behavior was observed, and it was more realistic. Different types of impact conditions were tested, and the model was stable in these conditions.

2 LITERATURE REVIEW

2.1 Fluid model in Whitfield's and Vasquez's TL-6 vehicle model

Researchers have done the investigation of the MASH TL-6 test vehicle in three phases. During the first phase, Whitfield developed the initial model for the MASH TL-6 test conditions [6]. The author's research focused on designing a barrier that can withstand a collision with a TL-6 vehicle (Tractor-tank trailer), contain the vehicle, and redirect it to safety minimizing damage.

In Whitfield's vehicle model, the fluid was modeled with pure Lagrangian solid elements (ELFORM=1). The properties of water were taken as; temperature was 20°C (72°F), density was 1.0E-6 kg/mm³, Poisson's ratio of 0.2, and a bulk modulus of 2.15 GPa.

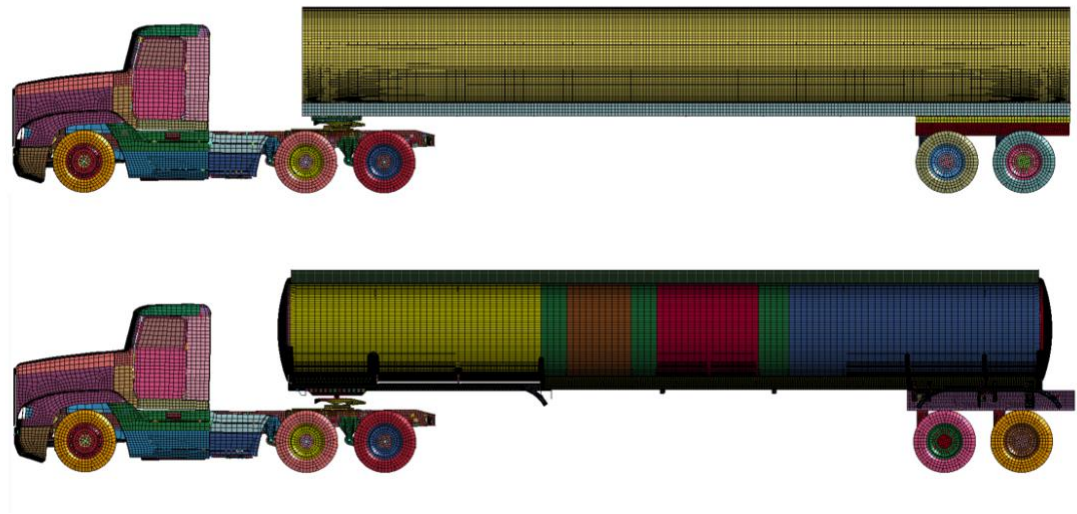


Figure 1. Whitfield's Model (Top) and Vasquez's Model (Bottom) [7].

Vasquez et.al. continued the research on the TL-6 vehicle model [7]. This time, researchers were mostly focused on the structural aspect of the vehicle model. However, they also performed a comparative study on different modeling approaches, such as.

Lagrangian, Eulerian, Smooth Particle Hydrodynamics (SPH), and Arbitrary Eulerian-Lagrangian (ALE). Upon studying computation time, robustness of models, and the stability of the model, they decided to use Whitfield's Lagrangian Elastic model of the fluid. Fluid modeled as an elastic body can serve to provide mass and momentum, but it was not adequate to predict the sloshing behavior of the fluid. Though the fluid model was used to predict the crashworthiness of various barrier shapes meant to contain the vehicle, the model of the fluid was not sufficiently stable to evaluate long contact and simulation intervals, post-impact vehicle stability, or trailer dynamics. Further improvements to model stability and accuracy were desired.

2.2 Incompressible Computational Fluid Dynamics (ICFD) in LS-DYNA

Simulation of a fluid-filled vessel involved in a structural collision is very numerically challenging. Most solid structures used in impact simulations are evaluated using traditional Finite Element Analysis (FEA) with Lagrangian element formulation, and sometimes meshless or Eulerian methods when deformations are very large. Collisions are usually very short duration, highly impulsive events. However, fluids are typically modeled using solvers that consider volumetric reactions spanning much longer timeframes than used in impacts.

The impact of fluid-filled tank results in dynamic changes between the interior contact structure and the fluid. Deformation of the bounding vessel is a nonlinear boundary condition for the fluid. To solve a nonlinear fluid contact problem, where the fluid is incompressible, the ICFD approach could be a solution.

LS-DYNA version 971 released the ICFD solver. It can solve the FEA of fluid dynamics, and it can be simultaneously coupled with the structural solver (Lagrangian)

together with an optional thermal solver. This allows researchers to investigate multiple domains of physical problems. It also allows researchers to investigate physical phenomena where two fluids of different densities (oil-air, water-air) are in effect. In this study, the thermal solvers were not included in the modeling.

The ICFD solver uses the Navier-Stokes equation combined with the continuity equation to solve incompressible fluid problems [8]. The combined equations are the governing equations to solve the incompressible fluid mechanics problems.

A fluid is assumed to be incompressible when the Mach number (M) is below 0.3 [8]. Where, Mach number is the ratio of Fluid velocity (V) to the velocity of sound in that fluid at that instance (C), described in equation (1).

$$M = \frac{V}{C} \quad (1)$$

The differential form of the continuity equation is as follows:

$$\frac{\partial \rho}{\partial t} + \nabla \cdot (\rho \vec{u}) = 0 \quad (2)$$

If density (ρ) is a constant in other words incompressible fluid, the mass continuity equation (2) simplifies to a volume continuity equation.

$$\nabla \cdot \vec{u} = 0 \quad (3)$$

The Navier stokes equation with the continuity equation has the following formulation, which is the governing equation for ICFD solver.

$$\rho \left(\frac{du_i}{dt} + u_j \frac{\partial u_i}{\partial x_j} \right) = \frac{\partial \sigma_{i,j}}{\partial x_j} + \rho f_i \quad \text{in } \Omega \quad (4)$$

$$\frac{\partial u_i}{\partial x_i} = 0 \quad \text{in } \Omega \quad (5)$$

The total stress tensor is given by,

$$\sigma_{ij} = -p\delta_{ij} + \mu \left(\frac{\partial u_i}{\partial x_j} + \frac{\partial u_j}{\partial x_i} - \frac{2}{3} \frac{\partial u_l}{\partial x_l} \delta_{ij} \right) \quad (6)$$

For incompressible flow, it is assumed that,

$$\frac{\partial u_i}{\partial x_i} \ll \frac{\partial u_i}{\partial x_j} \quad (7)$$

Considering Equation (7), the stress tensor, Equation (6) can be rewritten as:

$$\sigma_{ij} \approx -p\delta_{ij} + \mu \left(\frac{\partial u_i}{\partial x_j} + \frac{\partial u_j}{\partial x_i} \right) \quad (8)$$

Similarly, the momentum equation can also be simplified for the incompressible flow:

$$\begin{aligned} \frac{\partial \sigma_{ij}}{\partial x_j} &= -\frac{\partial p}{\partial x_j} \delta_{ij} + \frac{\partial}{\partial x_j} \left[\mu \left(\frac{\partial u_i}{\partial x_j} + \frac{\partial u_j}{\partial x_i} \right) \right] \\ &= -\frac{\partial p}{\partial x_j} \delta_{ij} + \mu \frac{\partial}{\partial x_j} \left(\frac{\partial u_i}{\partial x_j} \right) + \mu \frac{\partial}{\partial x_j} \left(\frac{\partial u_j}{\partial x_i} \right) \\ &= -\frac{\partial p}{\partial x_j} \delta_{ij} + \mu \frac{\partial}{\partial x_j} \left(\frac{\partial u_i}{\partial x_j} \right) + \mu \frac{\partial}{\partial x_i} \left(\frac{\partial u_j}{\partial x_j} \right) \\ &\approx -\frac{\partial p}{\partial x_j} \delta_{ij} + \mu \frac{\partial}{\partial x_j} \left(\frac{\partial u_i}{\partial x_j} \right) \end{aligned} \quad (9)$$

These simplifications change the governing system of equations (4), and (5) to the following system:

$$\rho \left(\frac{\partial u_i}{\partial t} + u_j \frac{\partial u_i}{\partial x_j} \right) = -\frac{\partial p}{\partial x_i} + \mu \frac{\partial^2 u_i}{\partial x_j \partial x_j} + \rho f_i \quad \text{in } \Omega \quad (10)$$

$$\frac{\partial u_i}{\partial x_i} = 0 \quad \text{in } \Omega \quad (11)$$

Different features of ICFD that are involved in this research, such as automatic volume meshing, level set, fluid-structure interaction (FSI), and coupling methods are discussed in the following sub-sections. These features are necessary to model the ICFD fluid model.

2.2.1 Automatic Volume Meshing- Delaunay Criterion

In the ICFD solver, the automatic volume mesher creates the fluid or air domain from the predefined surface nodes and elements. The initial fluid volume is created from the surface nodes and elements by satisfying the Delaunay criterion [8]. The Delaunay triangulation criterion is the fundamental basis of the formulation of Fluid volume mesh in ICFD solver. According to the Delaunay triangulation, there should not be any nodes present outside or inside the circumcircle of any triangular element created by a set of nodes, i.e., the other node should be exactly on the circumcircle of the first triangle, which is the circle connecting all the vertices. Delaunay triangulation is very useful for both two-dimensional and three-dimensional mesh generation [9].

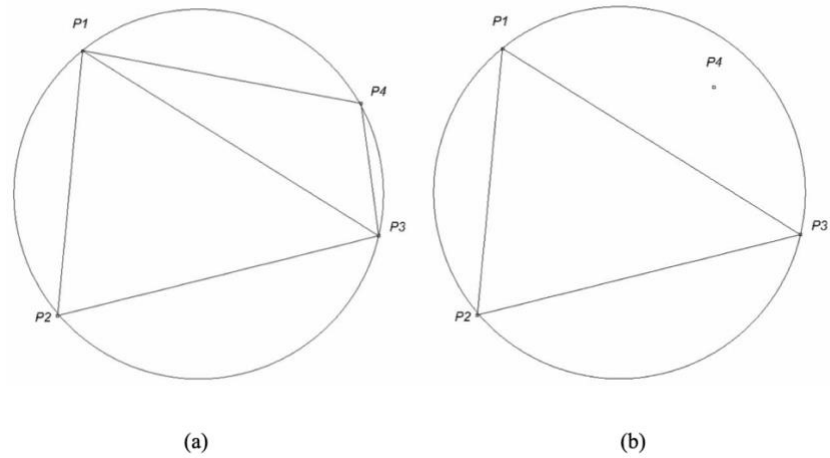


Figure 2. Delaunay criterion. a) Satisfied b) Violation

An example of the Delaunay criterion is shown in Figure 2(a), all the nodes P1, P2, P3, and P4 satisfy the Delaunay criterion, because they are on the same circumcircle. However, the nodes P1, P2, and P3 are on the same circumcircle, but P4 is not on the circumcircle for a violation of the Delaunay criterion, as shown in in Figure 2(b).

From the surface nodes, ICFD creates an initial volume mesh, then the ICFD solver progressively adds nodes to create the volume mesh in the fluid domains based on the Delaunay criterion. For this reason, it is crucial that the surface nodes don't have any overlapping surfaces, duplicate nodes, or any gaps between them.

2.2.2 Free surface- Level set method

Fluid problems with fixed volumes and container sizes require consideration of the moving interface of the fluid domain. As for this research, the air-water interface was a major part of the model. Many factors play important roles in interface modeling, such as density ratio, temperature difference, surface tension, and boundary conditions. The ICFD

solver uses a level-set method based on Osher et.al. [10], a fast reliable technique to track and correctly represent moving interfaces.

A conventional approach for defining an interface between distinct domains involves designating certain nodes to reside on the interface. The movement of these nodes is determined by the fluid velocity values across the grid, following a Lagrangian formulation. However, this becomes challenging when the interface element mesh undergoes significant changes or distortions. Consequently, frequent, and regular re-meshing becomes necessary for the distorted domain, incurring a substantial computational time cost. To overcome these issues, the ICFD solver adopts a level-set method to effectively track and represent evolving interfaces. The level set function, denoted as ϕ , serves as an implicit distance function subjected to a convection equation. The absolute value of ϕ represents the distance to the interface, with $\phi=0$ precisely at the interface, making it a Eulerian formulation [10]. The use of different signs indicates distinct sides of the interface. This level-set methodology proves advantageous in achieving more accurate simulations of interface dynamics. Figure 3 shows the adaptation of the level set in ICFD in a classical dam-breaking problem.

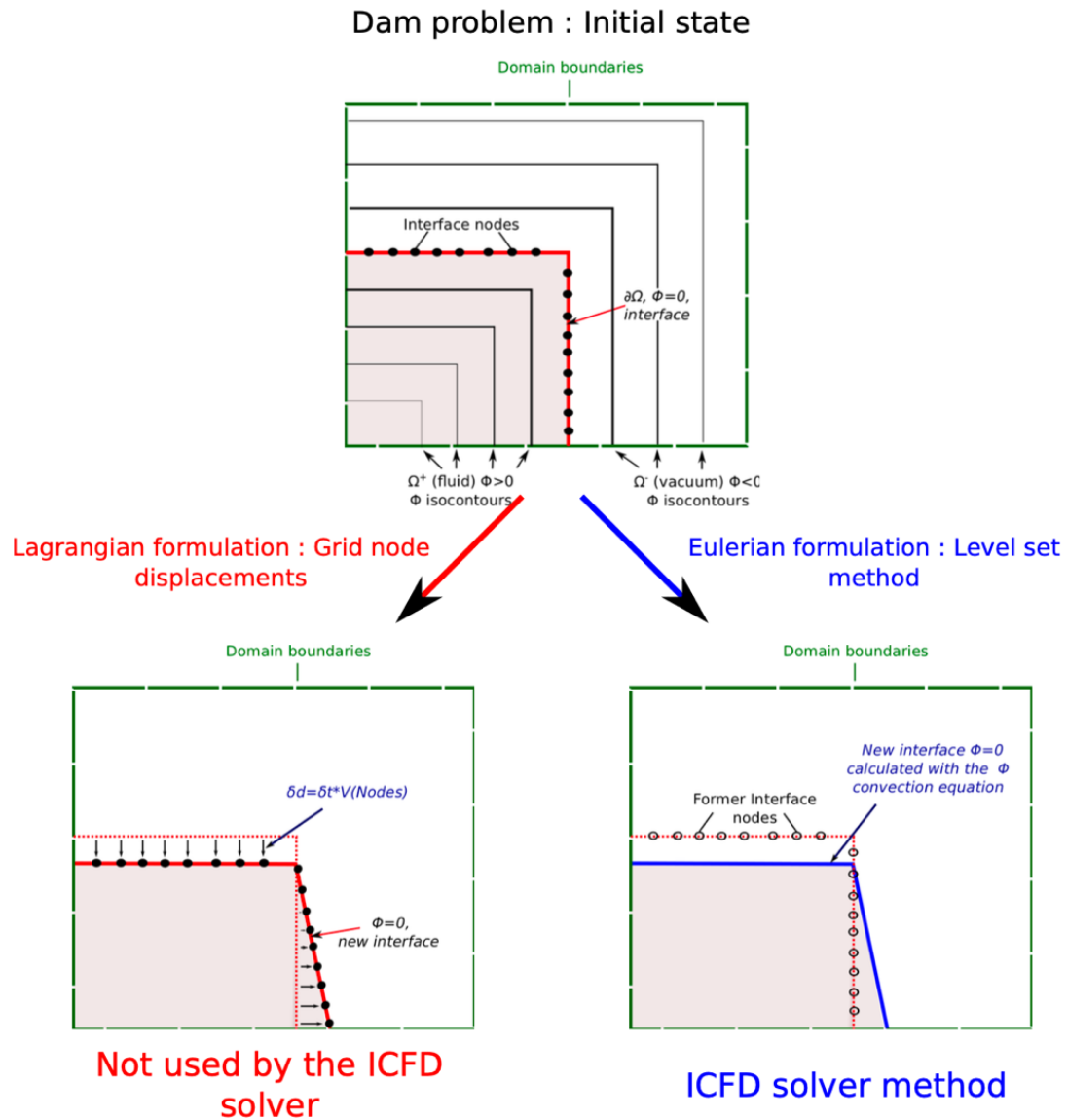


Figure 3. Different types of Level set methods [8].

2.2.3 FSI coupling methods in ICFD.

Another notable advantage of the ICFD solver is its capability to address fully coupled Fluid-Structure Interaction (FSI) problems. FSI involves the nonlinear interaction between a structure and an adjacent incompressible fluid. Historically, various methods have been used to solve FSI problems.

The monolithic approach treats the coupled problem of fluid and structure as a single domain, solving the equations of both fluid and structure simultaneously. However, this approach incurs high computational costs, as shown in Figure 4.

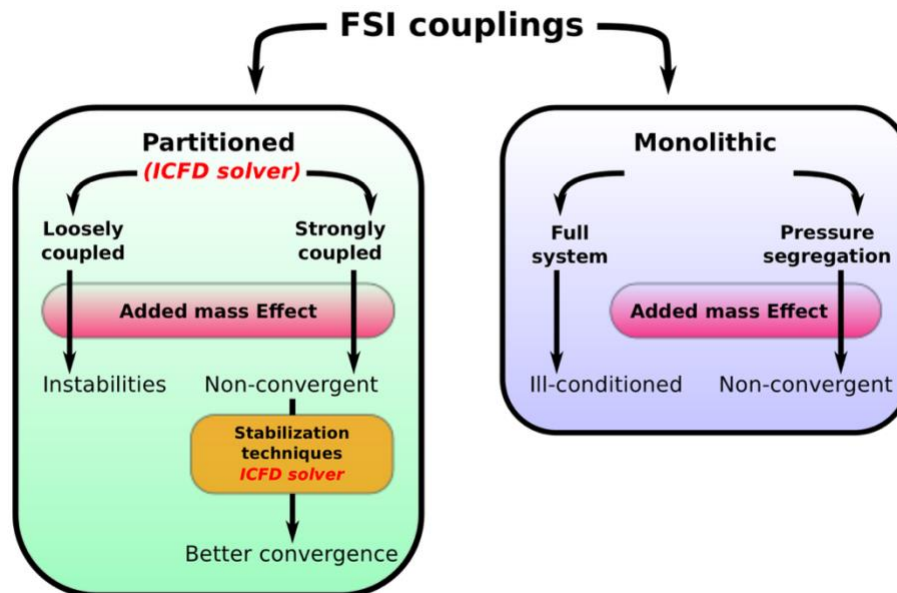


Figure 4. Two types of FSI coupling [8].

The partitioned method involves separating pressure from other unknowns in the monolithic approach, keeping computational costs lower. However, it necessitates solving the structure equations directly within the ICFD solver, which proves impractical. In contrast, the partitioned approach treats fluid and structure equations separately, breaking the system into partitions based on functional, physical, or computational considerations. The partitioned approach includes three directions on how to couple the interaction simulation programs, such as:

- **One-way coupling:** The fluid solver transfers stresses or loads to the solid solver only.

- **One-way coupling:** The solid solver transfers displacement to the fluid solver only.
- **Two-way coupling:** Loads and displacements are transferred across the FSI interface, solving the full non-linear problem.

While one-way coupling methods reduce computational cost and processor communication steps, they do not guarantee energy conservation at the interface. The numerical model presented in this thesis opts for two-way coupling. Two-way coupling further divides into a strongly coupled scheme (implicit) and a loosely coupled scheme (implicit-explicit) within the ICFD solver in LS-DYNA. The explicit solver is typically employed for dynamic structural deformation analyses, whereas the implicit solver is suitable for both static and dynamic analyses. The explicit scheme, also known as the central difference method, estimates the solution at time $(t + \Delta t)$ based on the solution at time (t) . In contrast, the implicit method solves a dynamic equilibrium equation at $(t + \Delta t)$ based on itself and the fluid solver's solution at time (t) . The explicit solver requires only one solution for each time step and does not necessitate the inversion of the stiffness matrix, making it computationally fast. Conversely, the implicit solver requires inverting the stiffness matrix once or more during a load/time step.

2.2.4 Boundary Conditions

There are many ICFD keywords available to define the boundary conditions for the fluid domain. Boundary conditions include boundary surface geometry, temperature, velocity, hydrostatic pressure, and viscosity of fluid. The free surface can be defined by,

the *MESH_INTERF keyword and the interaction between the fluid domain and structural domain can be defined by the *ICFD_BOUNDARY_FSI keyword.

The fluid dynamics modeling has another important aspect to be considered. The boundary of the fluid can be divided into two categories:

- Non-Slip boundary condition, and
- Free Slip boundary condition

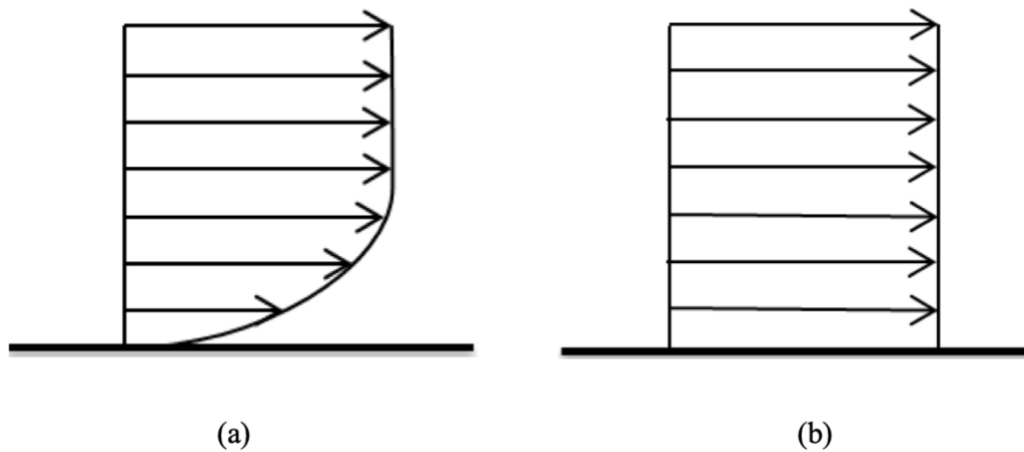


Figure 5. a) Non-slip Boundary condition, b) Free slip Boundary condition

This is due to the friction of the surface to the fluid. The non-slip condition occurs when the flow velocity at a flat surface is zero and gradually increases within the boundary layer. In contrast, the free-slip condition is characterized by a frictionless plane surface or when the fluid flows outside the boundary layer, where viscosity is neglected. Usually, this boundary condition is useful for modeling symmetric flow conditions. The velocity profile of the fluids in non-slip and free-slip conditions are shown in Figure 5. *ICFD_BOUNDARY_NONSLIP and *ICFD_BOUNDARY_FREESLIP keywords are available in the ICFD solver for the user to define these two boundary conditions.

2.3 Discussion

ICFD models are best suited for problems where there is a large volume of fluids involved and the fluid velocity is within the compressibility range, i.e., a maximum of one-third of the speed of sound in that medium. ICFD modeling is also very suitable when there are multiple non-mixable fluids involved. ICFD models are not suitable, when there is phase change of liquid to gas or gas to liquid at a very large quantity. ICFD models can be very stable and can predict the fluid behavior in different scales and conditions.

It was observed that in general, proper fluid models were not used in previous phases of the MATC TL-6 barrier development project. Fluids in the tank were modeled to have an elastic behavior. ICFD models were studied, and it is a better replacement than the previously used elastic fluid model. No one model works best in all situations; there are distinct advantages and disadvantages to each type of modeling. In future more detailed ICFD fluid model may offer a more accurate solution to the problem.

3 INITIAL FLUID DYNAMICS SIMULATION

3.1 2D fluid flow simulation over a cylinder

The first step in performing coupled ICFD interaction with a Lagrangian model of a structural collision was to evaluate limited models, calibrate based on available data, and confirm all interactions were modeled acceptably. A simple ICFD simulation was created consisting of a 2D fluid domain containing a circular obstacle. The problem represented a circular object immersed in a steady flow. It is to be noted that, in this simulation, only ICFD calculations were done, there was no FSI here.

3.1.1 Mesh generation

For this particular simulation, at first, a 10x15 rectangular geometry was made with a circle of 0.5 diameter inside. Since this was a 2D simulation, the elements for meshing were selected as 1D beam elements. The outer boundary was meshed with a coarser mesh and the circular edge was meshed with a finer mesh. The mesh on the leftmost edge was named part 1, right rightmost ones were part 2, the horizontal edges were named part 3, and the circular edge was named as part 4. The problem geometry is shown in Figure 6, in which part 1 is red colored, part 2 is blue colored, part 3 is green colored, and part 4 is purple colored.

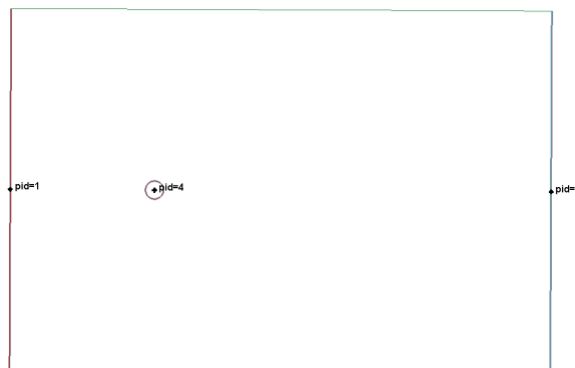


Figure 6. Geometry, Mesh, and Parts

For the ICFD modeling, it is preferable to generate the geometry and mesh first and then convert the mesh to Multiple Solver Mesh (MS Mesh). This MS mesh then acts as the surface mesh described in the previous chapter. After creating the mesh, it was converted to MS Mesh to perform ICFD analysis.

3.1.2 Model Setup

Preliminary assignments of parts and associated properties for the simple model described previously is shown in Figure 7.

```

*ICFD_SECTION
$#   sid
    1
*ICFD_MAT
$#   mid   flg   ro   vis
    1     1     1     1
*ICFD_PART
$#   pid   secid   mid
    1     1     1
*ICFD_PART
$#   pid   secid   mid
    2     1     1
*ICFD_PART
$#   pid   secid   mid
    3     1     1
*ICFD_PART
$#   pid   secid   mid
    4     1     1
*ICFD_PART_VOL
$#   pid   secid   mid
    10     1     1
$#   spid1   spid2   spid3   spid4
    1     2     3     4

```

Figure 7. Part, Material, Section cards of Example 1

The *ICFD_SECTION was defined, then *ICFD_MAT for material, the parameters were randomly selected (density and viscosity=1). Then all the parts were assigned with this *ICFD_SECTION and *ICFD_MAT. After that, the parts of the surface of the fluid domain were assigned with section and material information using *ICFD_PART_VOL card.

```

*MESH_VOLUME
$#  valid
    1
$#  pid1    pid2    pid3    pid4
    1        2        3        4
*MESH_BL
$#  pid    nelth
    4        1

```

Figure 8. Mesh cards of example 1

After the material properties are defined, the total fluid domain is created by the *MESH_VOLUME card in Figure 8. This keyword defines the volume space that the fluid will occupy maintaining the Delaunay Criterion as discussed previously. Care was taken, so that the boundary surfaces were non-overlapping, and didn't have any gaps or open spaces between them. The *MESH_BL defines the boundary layer for the mesh, it refines the volume mesh along the boundary of the user's choice, here it is along part 4.

```

*ICFD_BOUNDARY_PRESCRIBED_VEL
$#  pid    dof    vad    lcid
    1        1        1        1
*ICFD_BOUNDARY_PRESCRIBED_VEL
$#  pid    dof    vad    lcid
    1        2        1        2
*ICFD_BOUNDARY_PRESCRIBED_PRE
$#  pid    lcid    sf    death    birth
    2        2
*ICFD_BOUNDARY_FREESLIP
$#  pid
    3
*ICFD_BOUNDARY_NONSLIP
$#  pid
    4
*DEFINE_CURVE_TITLE
Velocity inlet
$#  lcid    sidr    sfa    sfo    offa    offo    dattyp
    1        1
$#  a1    o1
    0.0    1.0
    10000.0    1.0
*DEFINE_CURVE_TITLE
Pressure outlet
$#  lcid    sidr    sfa    sfo    offa    offo    dattyp
    2
$#  a1    o1
    0.0    0.0
    10000.0    0.0
*ICFD_DATABASE_DRAG
$#  pid
    4

```

Figure 9. Boundary, and Initial Conditions of Example 1

With *ICFD_BOUNDARY_PRESCRIBED_VEL a constant velocity of 1 was created at the inlet, i.e., leftmost edge. The rightmost edge was modeled as a constant pressure boundary with *ICFD_BOUNDARY_PRESCRIBED_PRE card. Free slip boundary condition was modeled on the horizontal edge with *ICFD_BOUNDARY_FREESLIP card. The circular edge was modeled as a non-slip boundary condition with *ICFD_BOUNDARY_NONSLIP card. These were the main components of the ICFD fluid model.

3.1.3 Results

After the calculation was completed, the fluid behavior was prominent in the fluid domain, there was visible vortex, and through a fringe plot, the change of velocity due to drag was observed from Figure 10 to Figure 12.

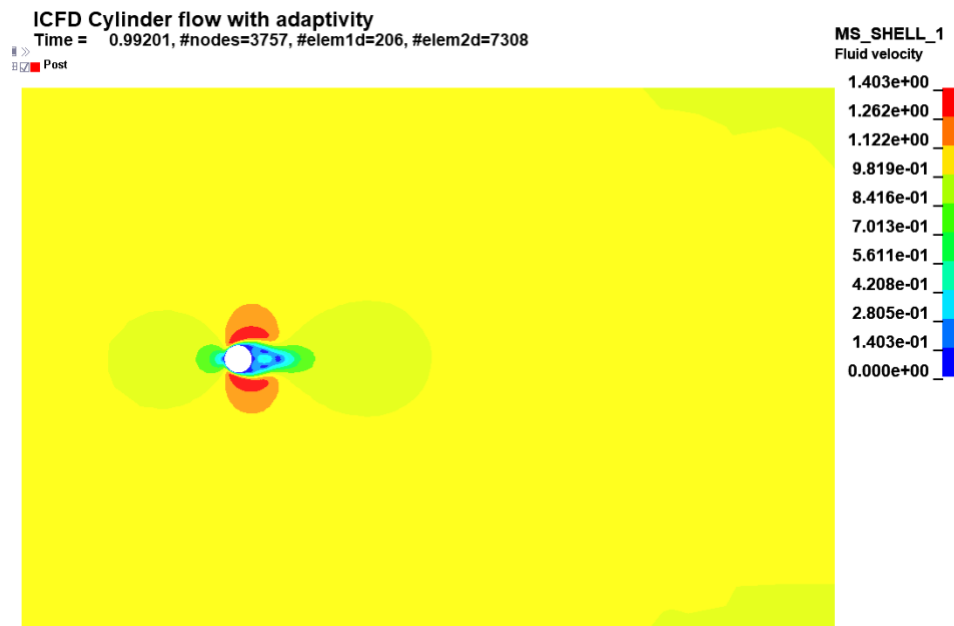


Figure 10. Results with velocity fringe plots of example 1

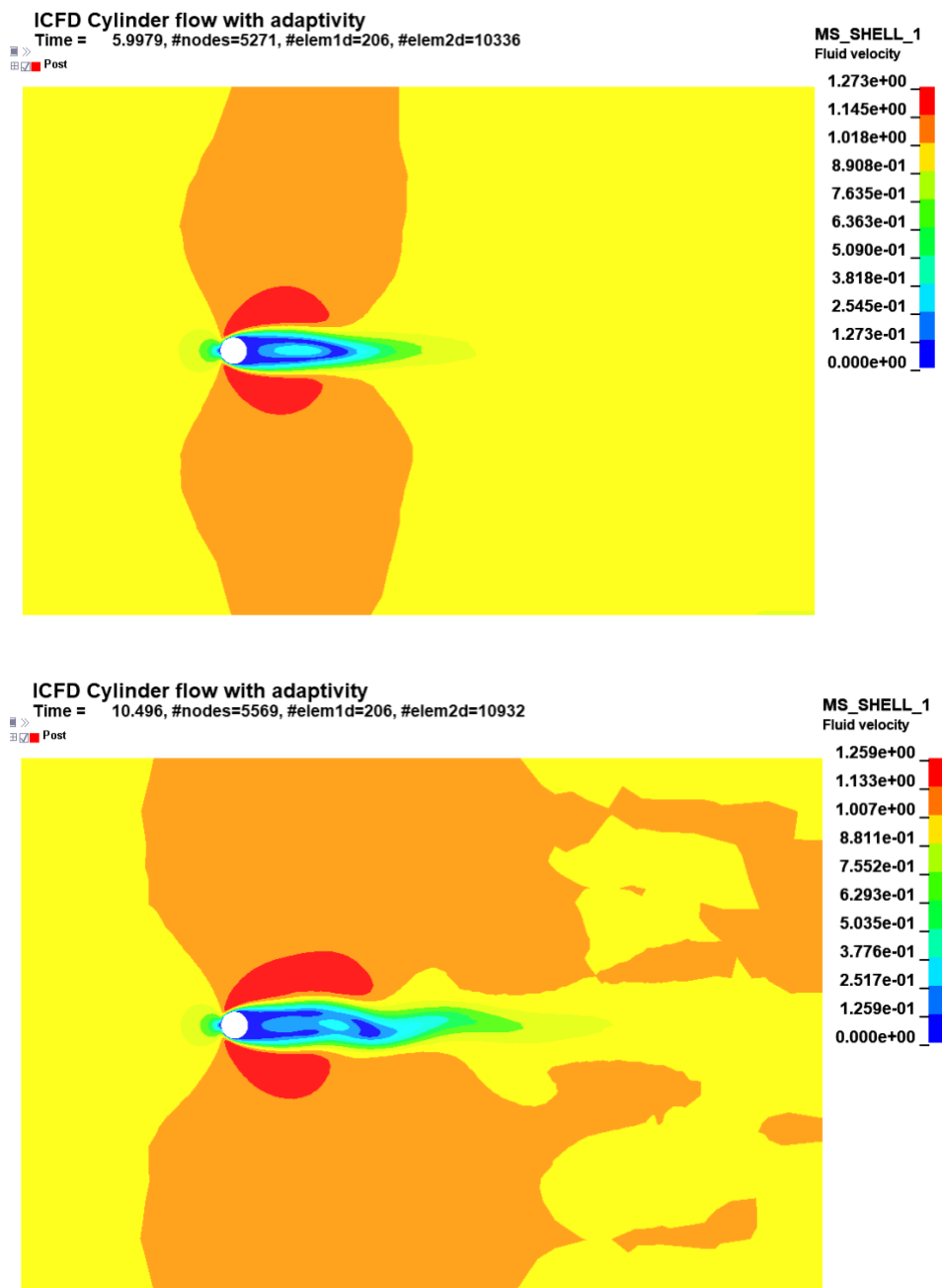


Figure 11. Results with velocity fringe plots of example 1(cont.)

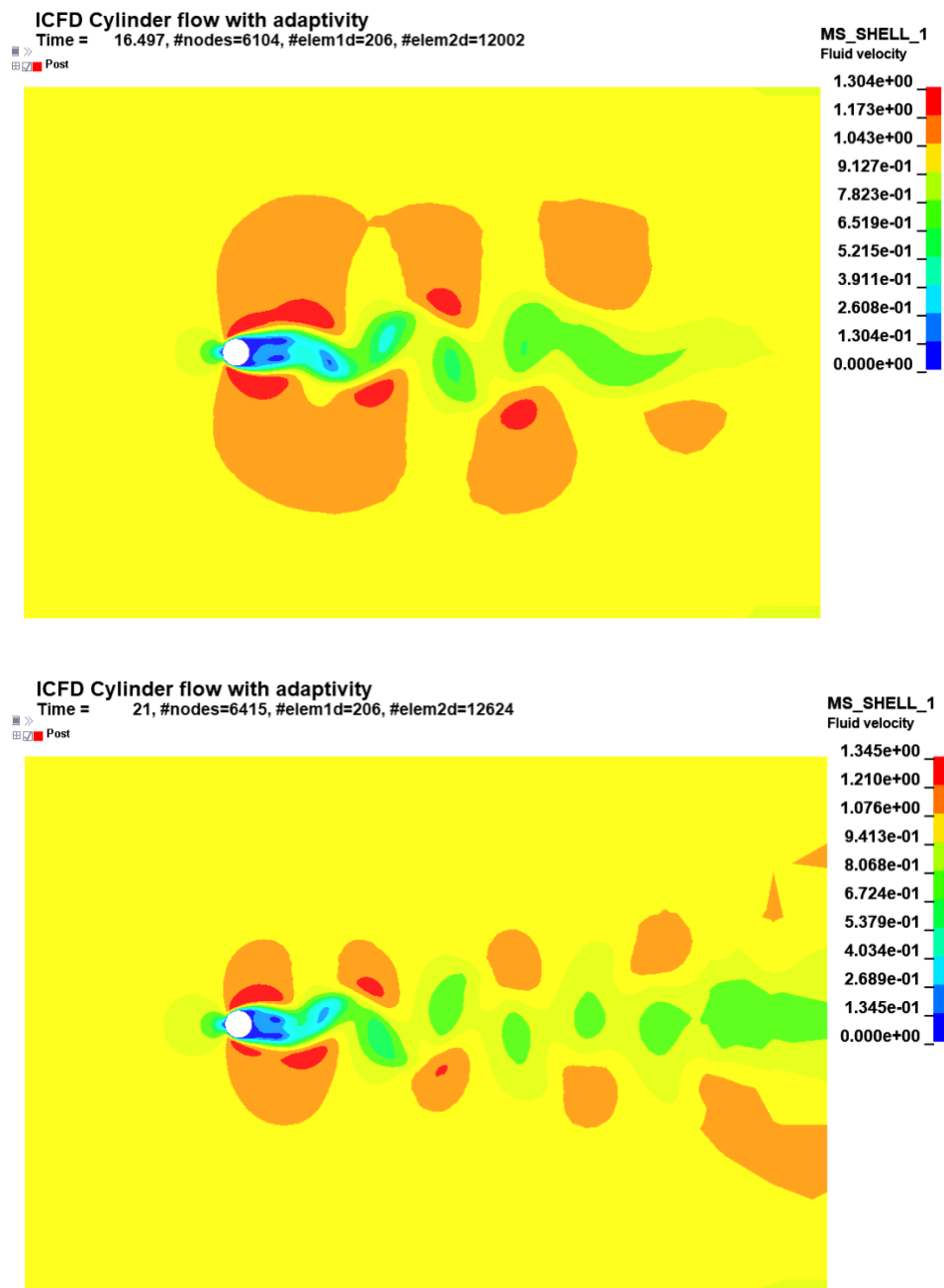


Figure 12. Results with velocity fringe plots of example 1(cont.)

Also, the mesh adaptation was confirmed. It can be seen in Figure 13 that, the mesh gets reformed with the change of time. Changes in the mesh were dynamic but subtle. Image headers indicated the number of elements in the model at each time step.

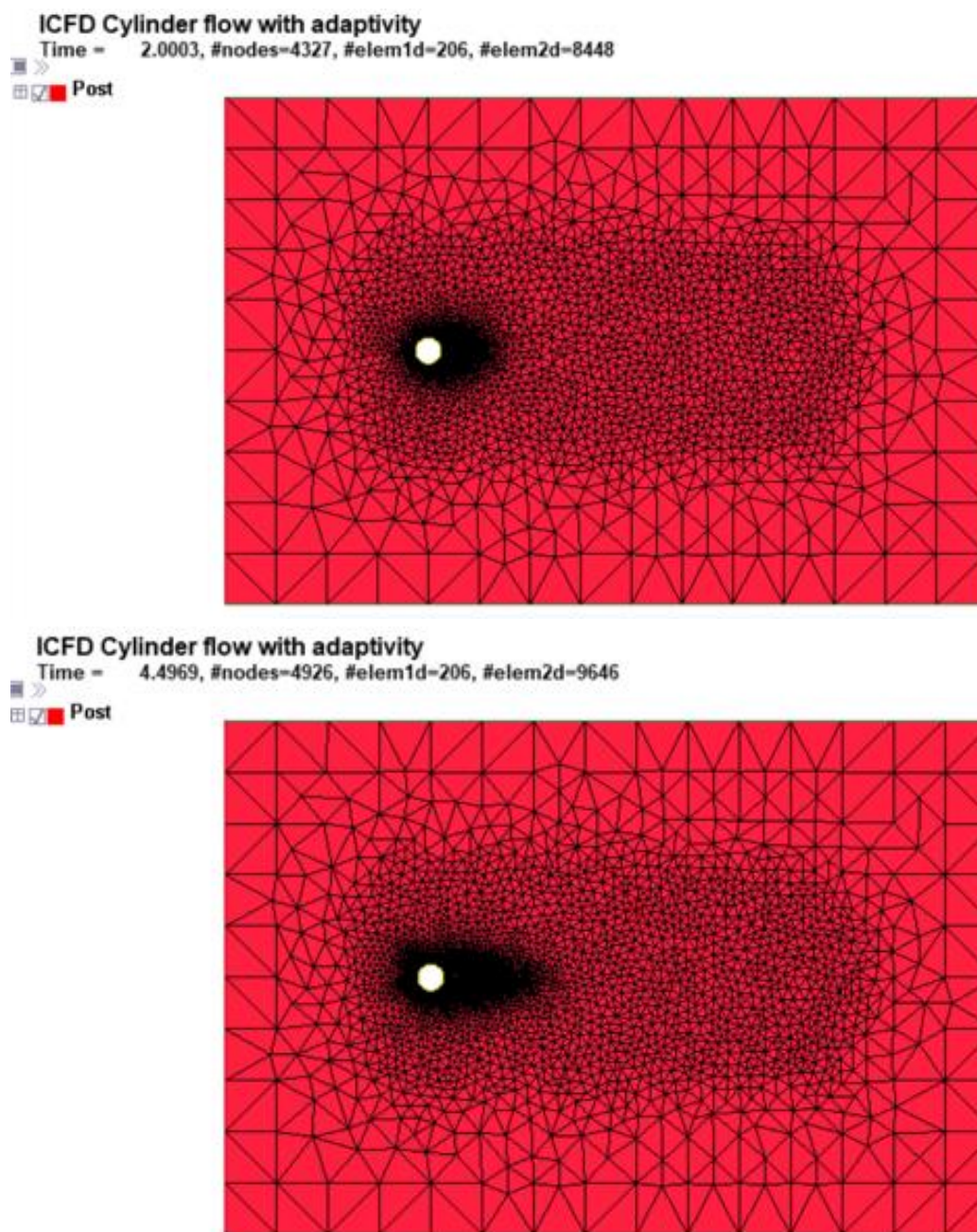


Figure 13. Mesh adaptation, Sequential image in example 1

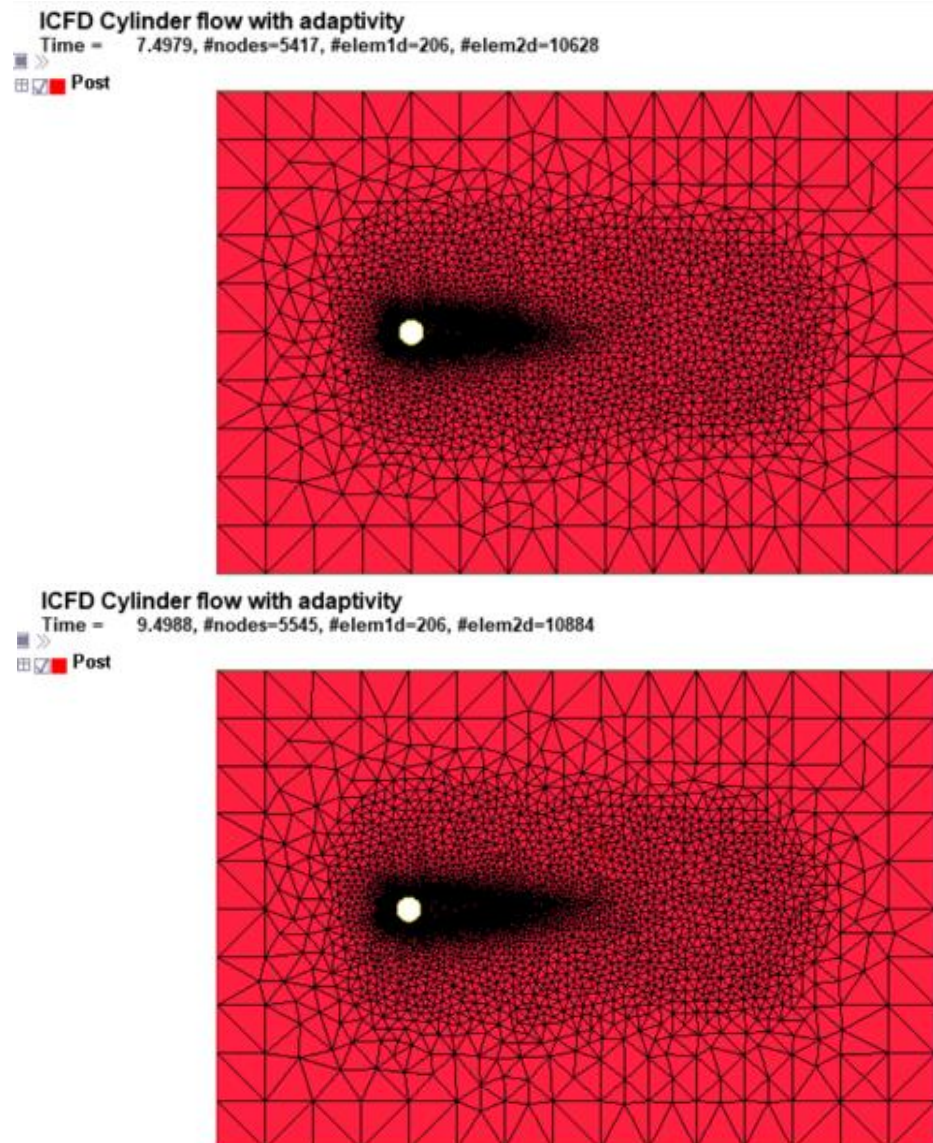


Figure 13. Mesh adaptation, Sequential image in example 1 (cont)

3.2 Fluid in a 3D container excited periodically

An additional example was generated with a more complex boundary condition. In this example, the fluid domain was modeled as the shape of a container, and the container was set to a back-and-forth motion using the *ICFD_CONTROL_IMPOSED_MOVE card. The motivation behind this simulation was to achieve the sloshing behavior of the fluid in a dynamic confined space, caused by externally applied force.

3.2.1 Mesh Generation and model setup

The Mesh generation techniques were almost the same as 2D, the only difference is that, here the surface parts were 2D triangular elements. For this model, a 1000 x 1000 x 1000 mm³ cuboidal shell geometry was created. The cuboidal shell was split into two different sections to model air and water. At their interfaces, another shell was created so that there were no physical gaps or overlaps between the surfaces. Then, the mesh was created, but in this case, the surfaces were meshed with triangular elements to satisfy the Delaunay Triangulation Criterion. This was similar to the procedure used with the 2D example. This step is very important for the ICFD modeling.

After the mesh was generated, it was converted to the MS Mesh, and the *ICFD_SECTION was defined as before. Since there are two materials involved, two *ICFD_MAT cards were defined. One of them had the properties of water (density 1e-6 kg/mm³, dynamic viscosity 1.005e-9 kg/mm-ms) with FLG= 1, which is for fully incompressible fluids. The other one was air, in ICFD, air is modeled as a vacuum, and for this the FLG=0 is sufficient.

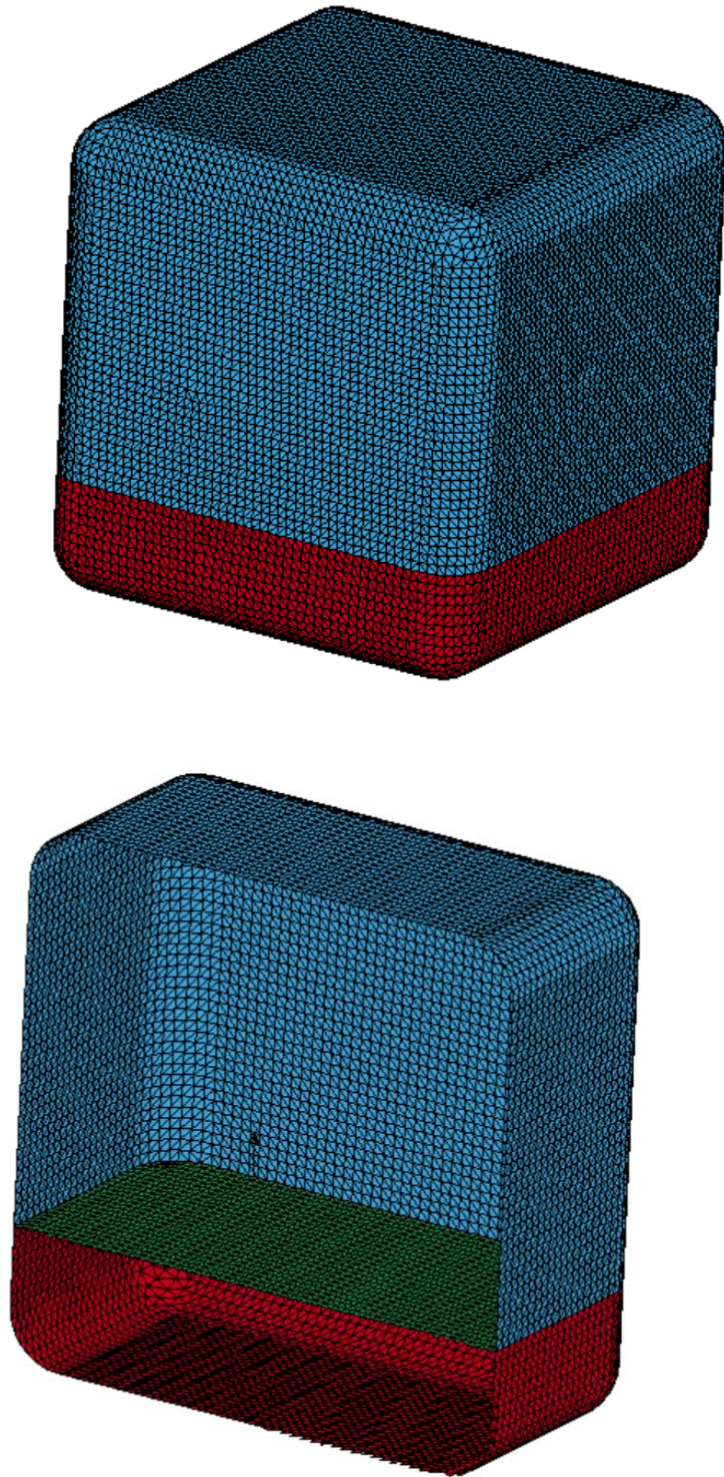


Figure 14. Mesh and parts of example 2. (Sectional view on the lower image)

The red part in Figure 14 is the boundary surface for water, the blue part is the boundary surface for the air and the green part is the interface between the air and water. The interface part was excluded from the *ICFD_PART_VOL card and the *MESH_VOLUME card since it was not a part of the boundary surface. The interface was defined using *MESH_INTERF card, this card creates the level set for the fluid interface. Since the whole fluid domain was surrounded by a container, all the surfaces were modeled with nonslip boundary conditions using the *ICFD_BOUNDARY_NONSLIP card. To excite the container periodically a curve was defined and then it was implemented at the *ICFD_CONTROL_IMPOSED_MOVE. This card moved the container back and forth to initiate sloshing behavior in the water.

3.2.2 Results

This model showed the sloshing behavior. The fringe plot on the level set showed the change of velocities, and the wave formation very well.

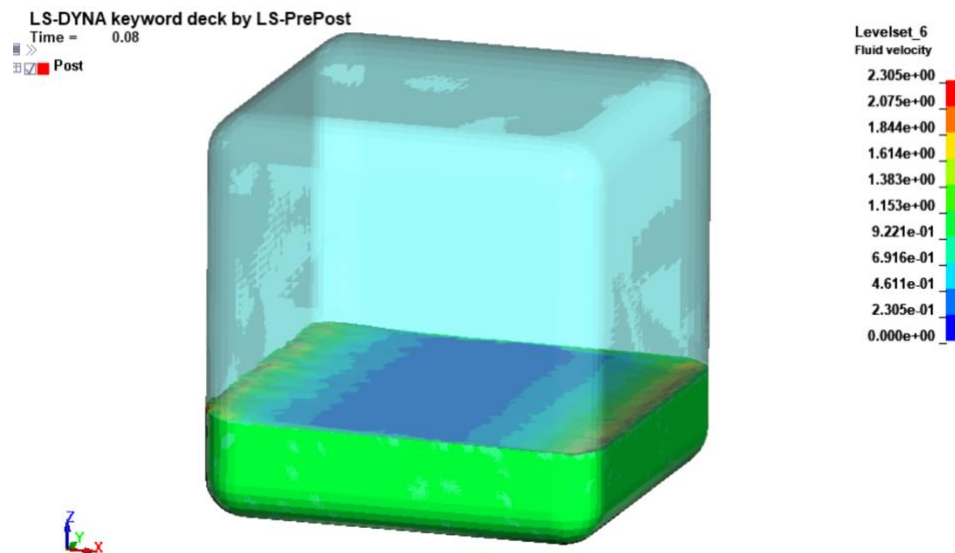


Figure 15. Sequential image of the simulation of example 2

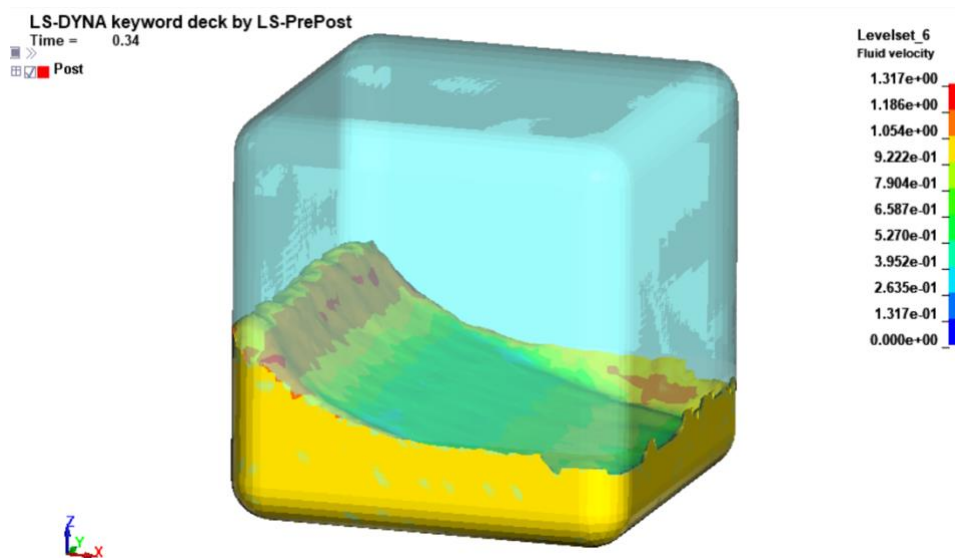


Figure 16. Sequential image of the simulation of example 2

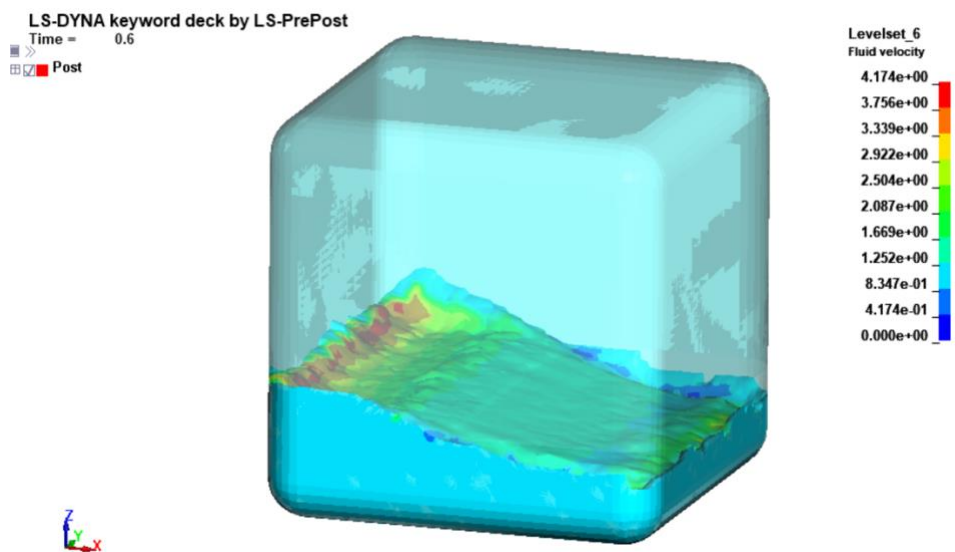


Figure 17. Sequential image of the simulation of example 2

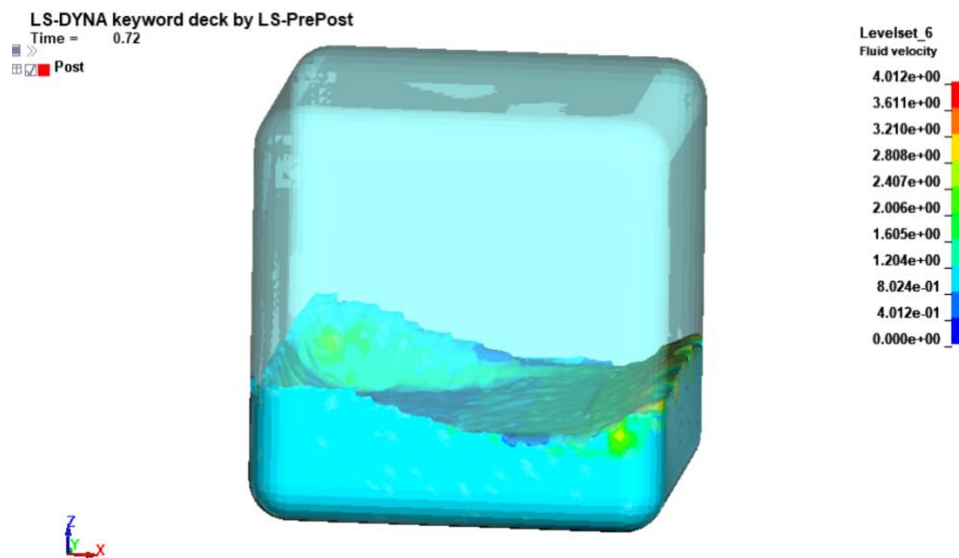


Figure 18. Sequential image of the simulation of example 2

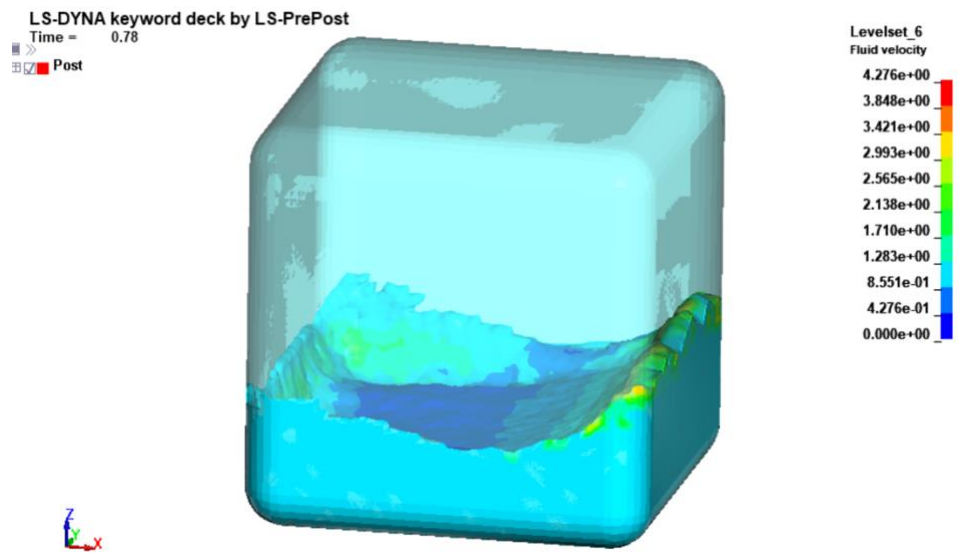


Figure 19. Sequential image of the simulation of example 2

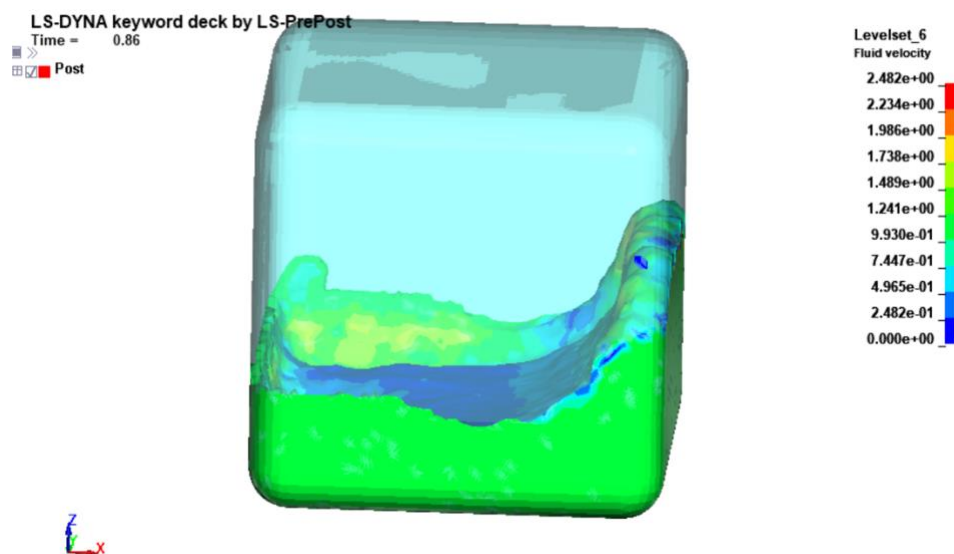


Figure 20. Sequential image of the simulation of example 2

As shown in Figures 15 to 20, stable sloshing behavior of the fluid in the container was achieved using an ICFD solution. Results suggest reasonable sloshing, and wave behavior of the fluid, which can be further verified by the work of Xue et.al. [11]. Their research shows a sloshing, and wave behavior of the fluid as this example showed in Figure 21 and Figure 22.

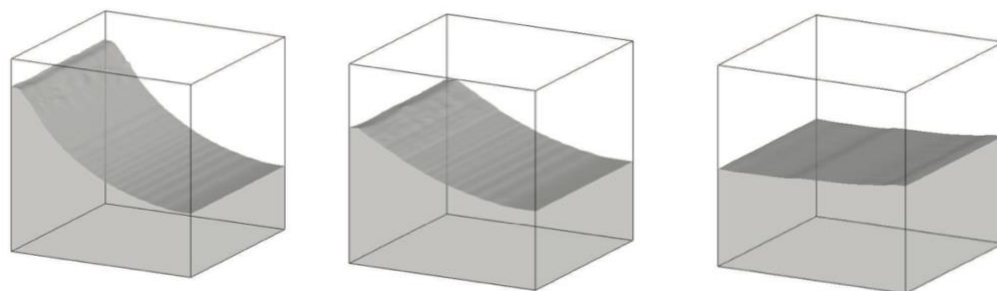


Figure 21. Sequential images of Fluid sloshing in Xue et.al. model [11].

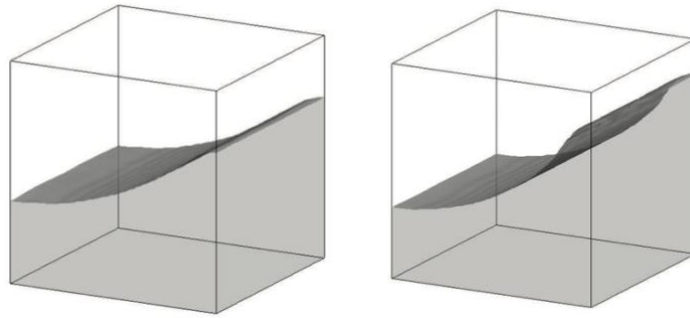


Figure 22. Sequential images of Fluid sloshing in Xue et.al. model [11]. (cont.)

3.3 FSI model simulation

In this example, a Fluid to Structure Interaction (FSI) problem was solved using ICFD. A water-flowing tunnel was modeled. In that tunnel, two flaps were placed to obstruct the flow of water. The flaps were modeled using shell elements and they had FSI encounter with the fluid domain. The motivation behind this example problem was to obtain a model that can exchange forces from the fluid volume, i.e., the ICFD solver to the flaps i.e., the structural solver.

3.3.1 Model Setup

To model this example, at first, the tunnel was created and then the flaps, the inlet surface, and the outlet surface were created. The left-most surface acted as the inlet side of the flow, where the boundary condition was set at a constant velocity, and the rightmost surface was the outlet of the flow having a zero-pressure boundary condition. Both boundary conditions were similar to that of the first example.

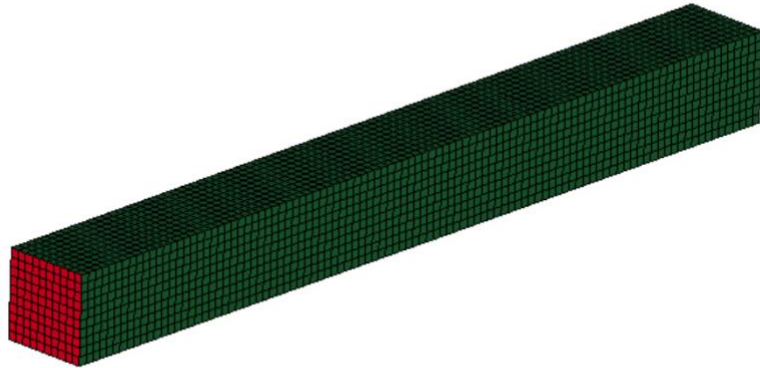


Figure 23. The model setup of example 3

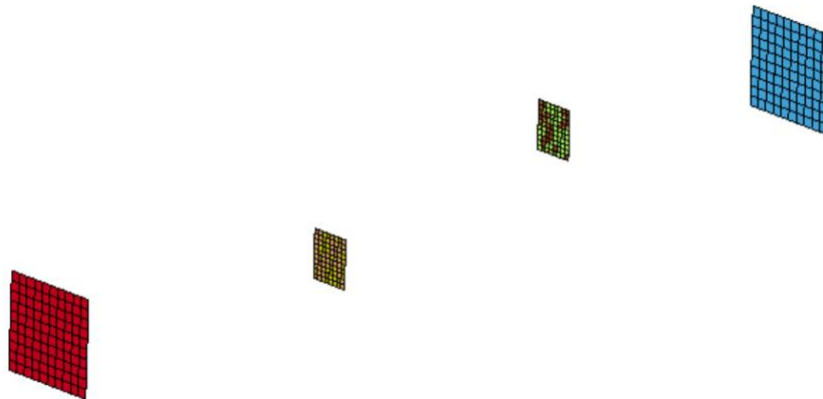


Figure 24. The model setup, hiding the sidewall, in example 3

This model created the necessity to introduce some new cards for FSI models and coupling between the fluid and the structural solver. To create FSI models in ICFD, it is widely accepted that the structural surfaces have also some ICFD surfaces, in this way it is easier to model the FSI interactions. For this reason, in most cases surfaces that go through the FSI have an overlapping structural and ICFD element. Since they are handled by two different solvers, this overlap does not create any issues. It can be observed in Figure 25

that, each flap has two colors of element, which indicates the presence of two overlapping elements.

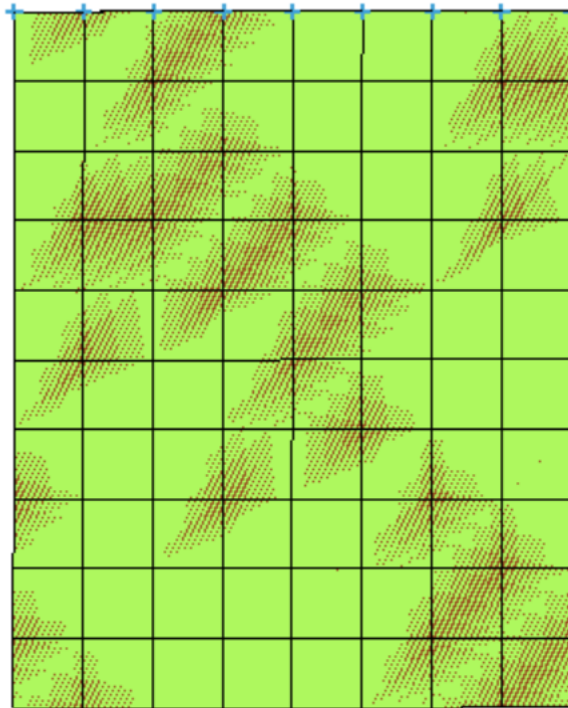


Figure 25. Overlapping elements at the FSI surface.

The ICFD surfaces that exchanged forces with the structural solver, were modeled as different part numbers to be called in the FSI cards, i.e., ICFD_BOUNDARY_FSI, and ICFD_CONTROL_FSI. The first card was used to define the surfaces in the fluid domain to establish FSI relations with the structural part. The second was used to trigger the FSI calculations. In the literature review, it was noted that for ICFD to properly model the fluid-structure interaction, there should not be any gaps in the fluid boundary surface elements. In this model, the fluid elements, that were used to overlap the flaps were not a part of the closed ICFD surface elements. This problem was addressed and solved by using the

*MESH_EMBEDSHELL card. This card treated the surfaces as if they were submerged in the generated fluid volume, having no role in the surface mesh. To refine the volume mesh along the FSI boundary *MESH_BL was used to define the number of elements near the surface that would act as a boundary layer.

The flaps were modeled as steel plates, having shell elements with ELFORM=16, and steel as the material. The end parts of the flaps were constrained with the help of the *BOUNDARY_SPC card. Additional LS-DYNA keyword inputs are shown in Figure 26.

```

*PART
$# title
flap 1
$#   pid   secid   mid   eosid   hgid   grav   adpopt   tmid
      44     44     44
*PART
$# title
flap 2
$#   pid   secid   mid   eosid   hgid   grav   adpopt   tmid
      55     44     44
*SECTION_SHELL
$#   secid  elform   shrf   nip   propt  qr/irid   icomp   setyp
      44     16      t3     3     nloc   marea    idof    edgset
$#   t1     t2     t4
      1.5
*MAT_ELASTIC
$#   mid   ro     e     pr     da     db   not used
      44   7.86E-6  200   0.30

```

Figure 26. Additional Inputs Required for FSI Example

3.3.2 Results

The model was stable, and the termination was normal indicating acceptable stability of the computations. For post-processing, a sectional plane was created after the simulation was performed. Upon observing the velocity profile, the turbulent behavior of the fluid created at the edge of the flaps was clearly visible as shown in Figure 27. The fluid velocity was reduced just behind the flaps and turbulent flow with vortices were observed.

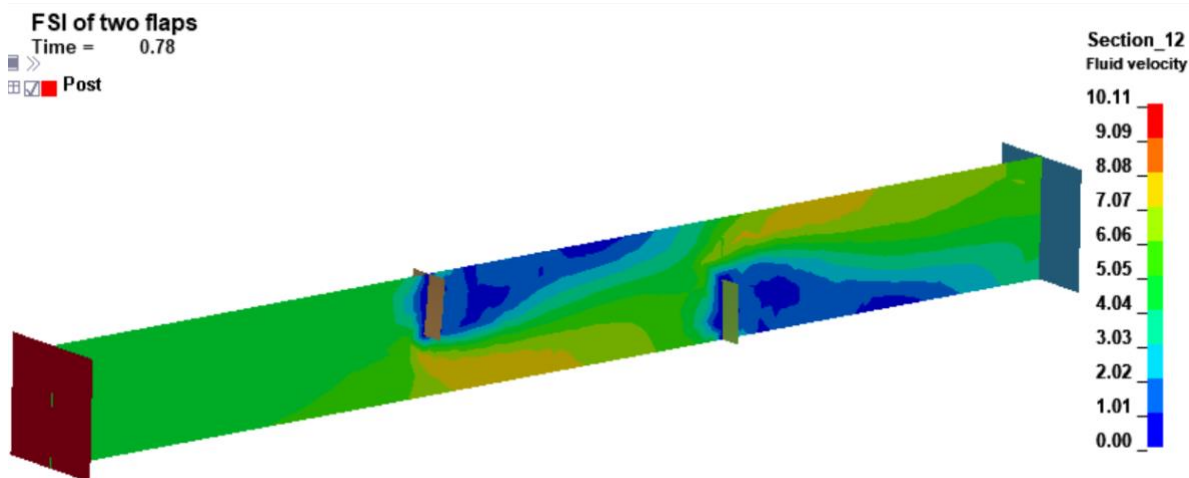


Figure 27. Fluid Velocity fringe plots around the flaps

A detailed inspection of the elastic flap models revealed that the fluids deformed the surfaces, as shown in Figure 29. Deformations of the elastic flaps were expected as a result of high fluid pressures. The peak pressure on the flaps was 8.4 MPa and the maximum displacement at the free end of the flaps was 53.4 mm on the left flap, shown in Figure 28.

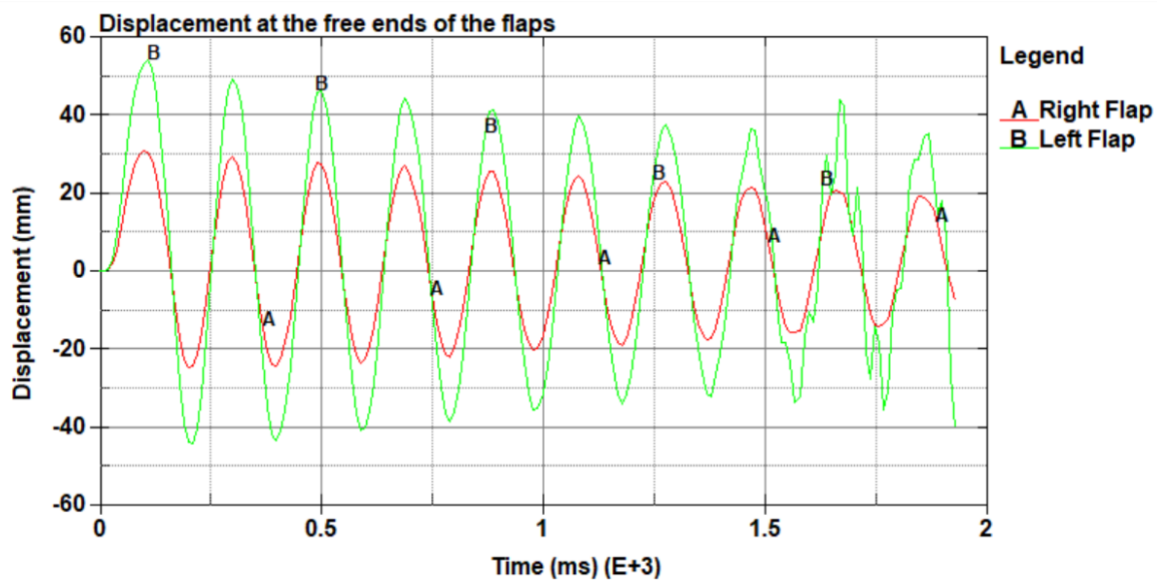


Figure 28. The displacement at the free ends of the flaps.

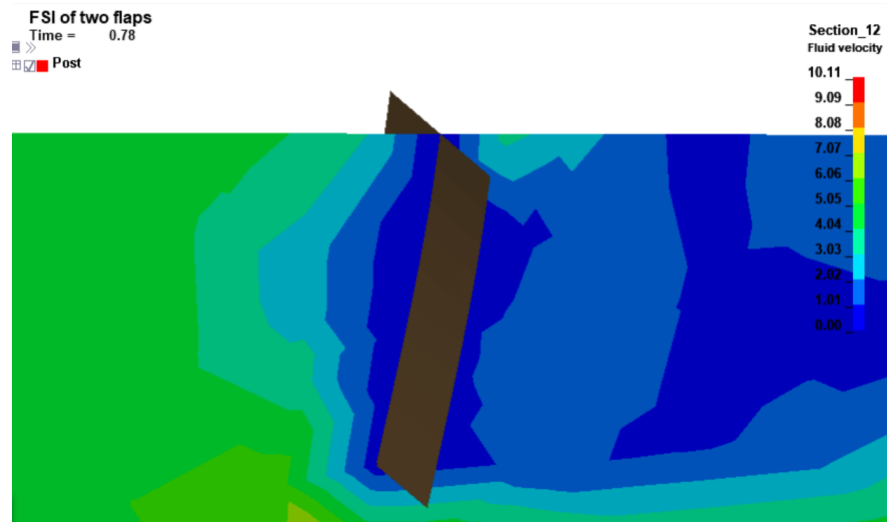


Figure 29. Deformation in the flaps due to fluid flow

For further investigation, the Von Mises stress profiles on the flaps were observed. It can be seen from Figure 30, that the first flap from the inlet of the flow (the left one in Figure 30), has higher stress concentration along the SPC boundary. The second flap also had stress concentration along the SPC edge but lesser, due to receiving a reduced fluid flow hence pressure, which is shown in Figure 31.

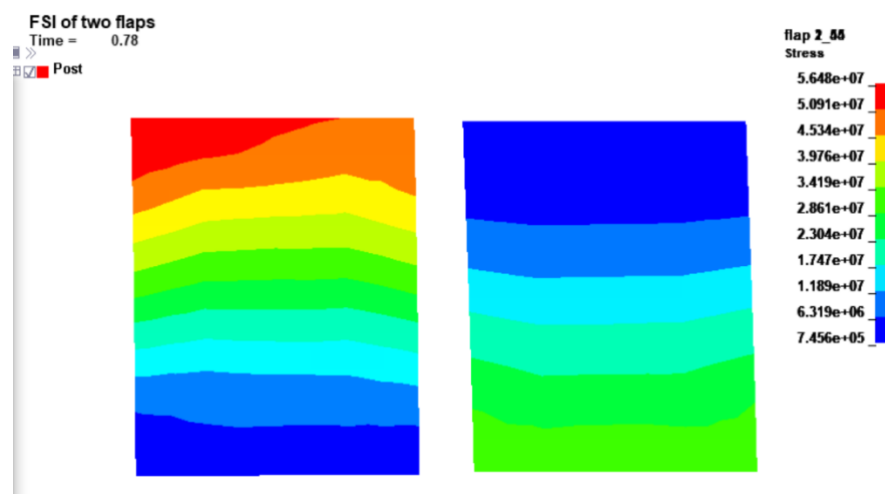


Figure 30. Stress profiles in the flaps. (Von Mises Stress)

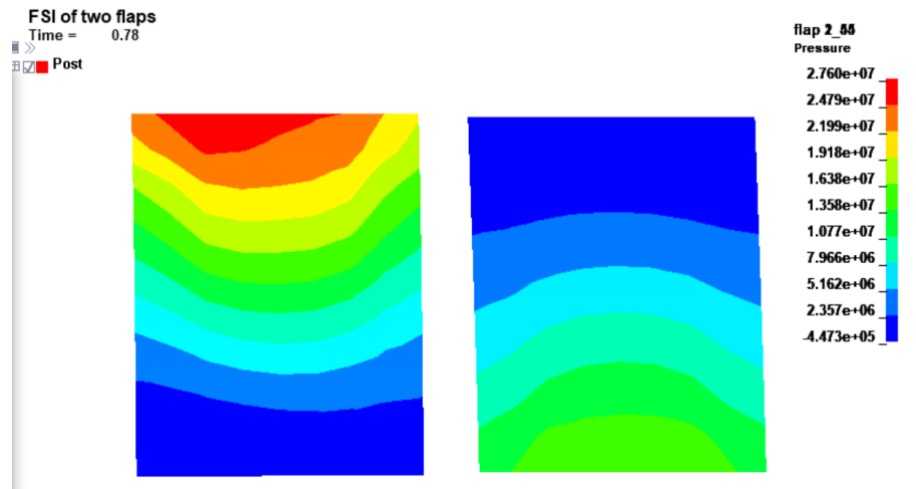


Figure 31. The pressure profile on the flaps.

4 ICFD-FSI MODEL FOR A DEFORMABLE CONTAINER

4.1 Introduction

A more challenging fluid-structure problem involving a Lagrangian external mesh containing an ICFD fluid and involved in an impact was simulated. The main objective was to achieve a deformable container model partially filled with water as ballast, capable of impacting some objects and deforming dynamically. For this study, an ICFD FSI model was created, and the impact was performed perpendicularly to a rigid wall.

4.2 Model details

4.2.1 The deformable container model

At first, a cylindrical capsule of 2m in length and 1m in diameter was created. It had a similar shape to the TL-6 vehicle's tanker. This scaled-down geometry was then modeled with rectangular shell elements having an element size of 20 mm. Some of the model inputs are shown in Figure 32.

```

$
*PART
$#
Container shell
$# pid secid mid eosid hgid grav adpopt tmid
    100 100 100 0 0 0 0 0
$
$
*SECTION_SHELL
$# secid elform shrf nip propt qr/irid icomp setyp
    100 2 1.0 5 1.0 0 0 1
$# t1 t2 t3 t4 nloc marea idof edgset
    3.0 3.0 3.0 3.0 0.0 0.0 0.0 0
$
$
|MAT_PIECEWISE_LINEAR_PLASTICITY
$# mid ro e pr sigy etan fail tdel
    1007.86000E-6 200.0 0.28 0.326 0.01.00000E21 0.0
$# c p lcss lcsr vp
    40.0 5.0 0 0 1.0
$ plastic stress strain curve
$# eps1 eps2 eps3 eps4 eps5 eps6 eps7 eps8
    0.0 0.0152 0.0226 0.0407 0.0691 0.0983 0.1345 0.7093
$# es1 es2 es3 es4 es5 es6 es7 es8
    0.326 0.328 0.3788 0.4414 0.497 0.53 0.5557 0.7604
$

```

Figure 32. Model inputs for cylindrical capsule

The shell elements were modeled with `*SECTION_SHELL`, having a thickness of 3 mm, `ELFORM=2`, and the number of integration points was 5. The material model was adopted from the TL-6 vehicle model developed by researchers at the Midwest Roadside Safety Facility at the University of Nebraska-Lincoln [12]. This is a steel model, modeled with the `*MAT_PIECEWISE_LINEAR_PLASTICITY` card, having a density of 7.86×10^{-6} kg/mm³, and Young's modulus of 200 GPa, Poisson's ratio of 0.28, and Yield strength of 0.326 GPa. An initial velocity of 20 m/s to the positive x-axis was assigned to the whole container using the `*INITIAL_VELOCITY_GENERATION` card. A rigid wall was modeled for the container to be impacted using `*RIGIDWALL_PLANAR`.

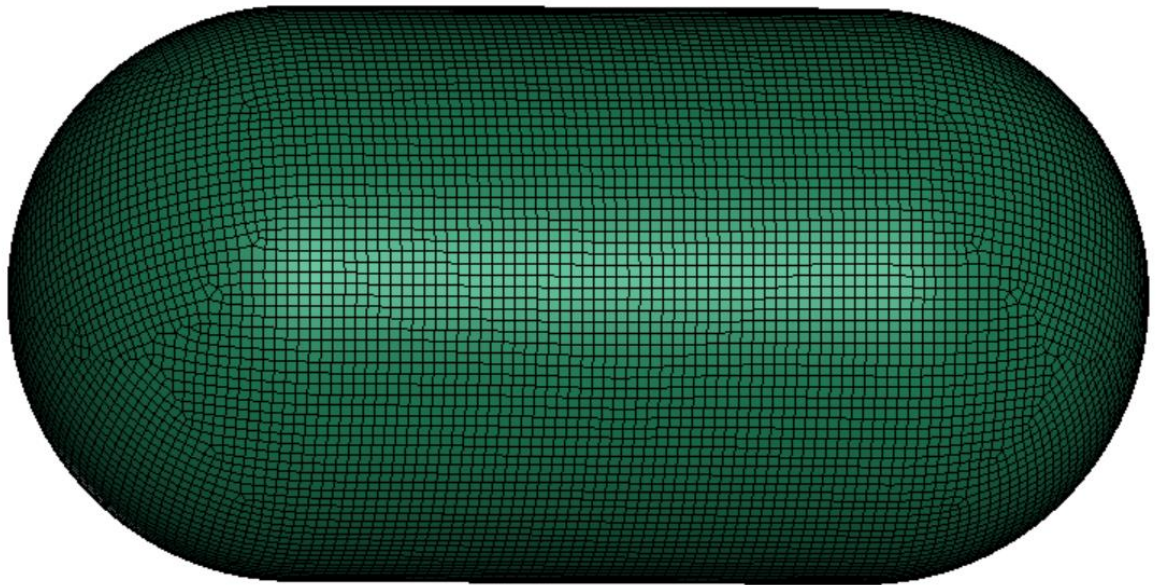


Figure 33. The deformable container model.

4.2.2 The ICFD model for the container

For the ICFD modeling, the same geometry was used as the container model. For the surface elements model, the water level was modeled at 715 mm height from the bottom

surface. The rest of the container was modeled as air, i.e., vacuum as described in example 2. The surface elements were generated as triangular shell elements, having an element size of 20 mm. The interface was also modeled with similar triangular shell elements. The surface elements are shown in Figure 34 and Figure 35. Care was taken so that there were no gaps or overlapping elements of the same type. It is to be mentioned that the final model has overlapping elements, but they are not the same type i.e., one being the structural element, the other being the ICFD element.

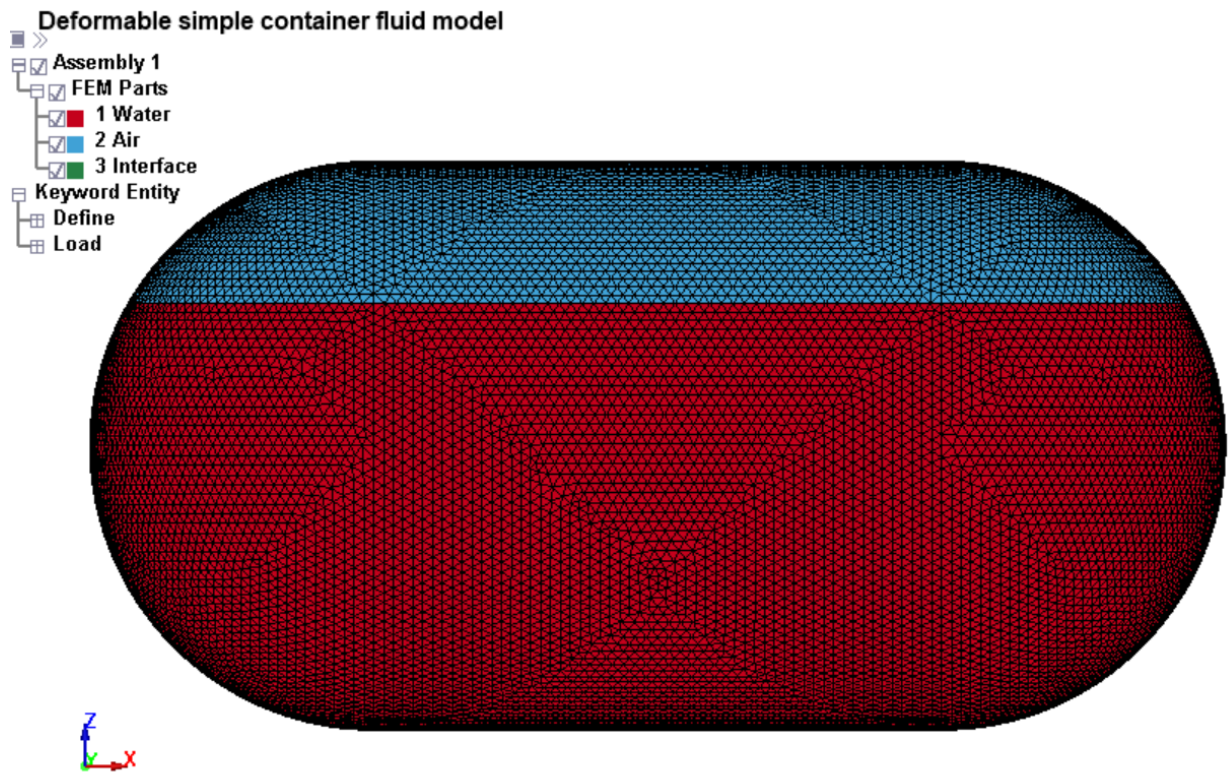


Figure 34. Surface elements of the deformable container model

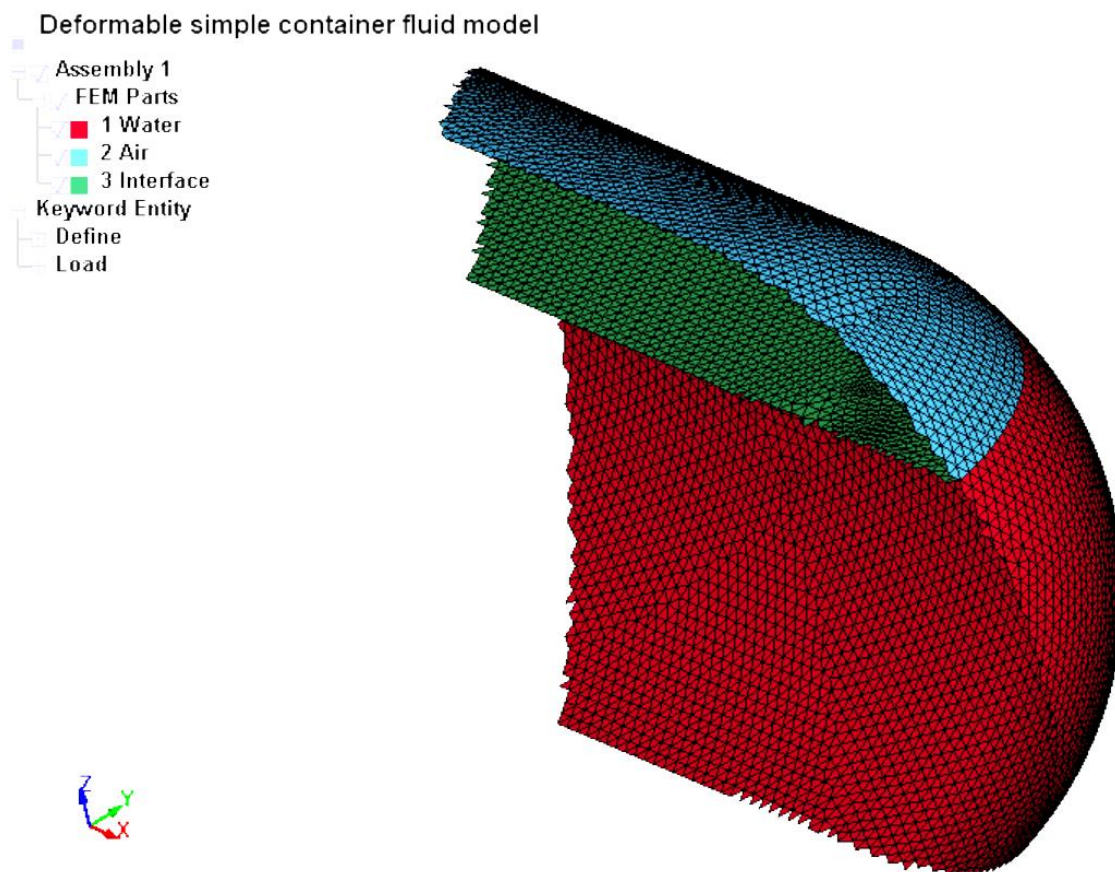


Figure 35. Cross-sectional view of the surface elements of the deformable container

The ICFD keywords used for this model are shown in Figure 36.

```

*ICFD_PART_TITLE
Water
$#   pid   secid   mid
      1     1     1
*ICFD_PART_TITLE
Air
$#   pid   secid   mid
      2     1     2
*ICFD_PART_TITLE
Interface
$#   pid   secid   mid
      3     1     1
*ICFD_PART_VOL
$#   pid   secid   mid
     10     1     1
$#   spid1  spid2  spid3  spid4  spid5  spid6  spid7  spid8
      1     3     0     0     0     0     0     0
*ICFD_PART_VOL
$#   pid   secid   mid
     20     1     2
$#   spid1  spid2  spid3  spid4  spid5  spid6  spid7  spid8
      2     3     0     0     0     0     0     0
*ICFD_SECTION
$#   sid
      1
*ICFD_MAT
$#   mid   flg     ro     vis     st  stsflcid   ca
      1     11.00000E-61.00500E-9  0.0  0  0.0
*ICFD_MAT
$#   mid   flg     ro     vis     st  stsflcid   ca
      2     0     0.0  0.0  0.0  0  0.0
*MESH_INTERF
$#   volid
     10
$#   pid1  pid2  pid3  pid4  pid5  pid6  pid7  pid8
      3     0     0     0     0     0     0     0
*MESH_VOLUME
$#   volid
     10
$#   pid1  pid2  pid3  pid4  pid5  pid6  pid7  pid8
      1     2     0     0     0     0     0     0

```

Figure 36. Model inputs for ICFD-capsule problem

4.2.2 ICFD and FSI controls and other cards

This model has an interaction between the ICFD solver and the Structural solver. For this reason, the FSI controls are necessary. In this model, the air and the water both had FSI interactions to them. In *ICFD_BOUNDARY_FSI, both surface parts were called, and the parts of the structural solver were called in *ICFD_CONTROL_FSI card. It is to be noted that in *ICFD_CONTROL_FSI card, the OWC value was chosen as 0, this will result in contact of the FSI boundary with all the available structural parts. The resulting controls of the mode are shown in Figure 37.

```

*ICFD_BOUNDARY_FSI
$#   pid
      1
      2
*ICFD_CONTROL_FSI
$#   owc      bt      dt      idc      lcidsf      xproj
      0      0.01.00000E28      0.25      0      0
$#   nsub
      0

```

Figure 37. FSI control inputs

Besides the FSI controls, there were some other ICFD controls used in this model.

*ICFD_CONTROL_TIME was used to fix the total run time of the simulation.

*ICFD_CONTROL_ADAPT_SIZE was used to create the adaptive meshing feature. Since there are plenty of movements in the ICFD fluid volume,

*ICFD_CONTROL_MESH_MOV card was picked to define how should the mesh move alongside the structural components. Mesh Motion Selector (MMSH) was picked as EQ.

2, which will result in moving the mesh by solving a linear elasticity approach solving the element sizes as stiffness. The *ICFD_DATABASE_AVERAGE, the

*ICFD_DATABASE_DRAG, and the *ICFD_DATABASE_FLUX cards were used to printout the average velocity, pressure, drag, and flux information from the simulation. The

additional ICFD control cards used in the capsule impact simulation are shown in Figure

38.

```

*ICFD_CONTROL_TIME
$#   ttm      dt      cfl      lcidsf      dtmin      dtmax      dtinit      tdeath
     100.0    0.0     1.0           01.00000E-91.00000E28      0.01.00000E28
*ICFD_CONTROL_ADAPT_SIZE
$#   asize      nit
     1         10
*ICFD_CONTROL_MESH_MOV
$#   mmsh  lim_iter  reltol
     2      100     0.001
*ICFD_DATABASE_AVERAGE
$#   dt
     5.0
*ICFD_DATABASE_DRAG
$#   pid      cpid      dtout      perout      divi      elout      ssout
     1         0         0.0         0          10         0         0
*ICFD_DATABASE_FLUX
$#   pid      dtout
     1         5.0

```

Figure 38. Additional ICFD control cards used in capsule simulation.

Since the structural part has the initial velocity generation card, the *ICFD_INITIAL card was not used. Using both initial velocity conditions made the model unstable. This will be discussed in a later section of this chapter.

Another important aspect of ICFD modeling is that ICFD calculations require implicit analysis. Though the usual practice for large deformation models is to perform explicit analysis, the ICFD models do implicit analysis by default. Some of the control cards were selected for the structural solver to make easier coupling. Among them, the *CONTROL_IMPLICIT_AUTO, the *CONTROL_IMPLICIT_DYNAMICS, the *CONTROL_IMPLICIT_GENERAL, and the *CONTROL_IMPLICIT_SOLUTION were used in this model. Implicit and explicit time analysis model controls are summarized in Figure 39.

```

*CONTROL_IMPLICIT_AUTO
$#  iauto  iteopt  itewin  dtmin  dtmax  dtexp  kfail  kcycle
    1     100     20     0.0   -700     0.0     0       0
*CONTROL_IMPLICIT_DYNAMICS
$#  imass  gamma  beta  tdybir  tdydth  tdybur  irate  alpha
    1     0.55  0.27563  0.01.00000E281.00000E28  1     0.0
*CONTROL_IMPLICIT_GENERAL
$#  imflag  dt0  imform  nsbs  igs  cnstn  form  zero_v
    1     0.1  2       0     1     0     0     0
*CONTROL_IMPLICIT_SOLUTION
$#  nsolvr  ilimit  maxref  dctol  ectol  rctol  lstol  abstol
    12     11     15     0.001  0.01  0.0     0.01.00000E-20
$#  dnorm  diverg  istif  nlprint  nlnorm  d3itctl  cpchk
    2     1     1     3     2     10     0
$#  arcctl  arcdir  arclen  arcmt  arcdmp  arcpsi  arcalf  arctim
    0     0     0.0     1     2     0.0     0.0     0.0
$#  lsmt  lsdir  irad  srad  awgt  sred
    5     2     0.0     0.0     0.0     0.0

```

Figure 39. Implicit model controls for coupled implicit-explicit model solutions.

The detailed keywords for this model is given in the Appendix.

4.3 Impact Simulation Results

The model successfully completed the simulation of impacting a rigid wall with an initial velocity of 20m/s. The gravity was in effect, so the container was allowed to free fall after the impact. The sequential images of the simulation with level sets are shown from Figure 40 to Figure 43.

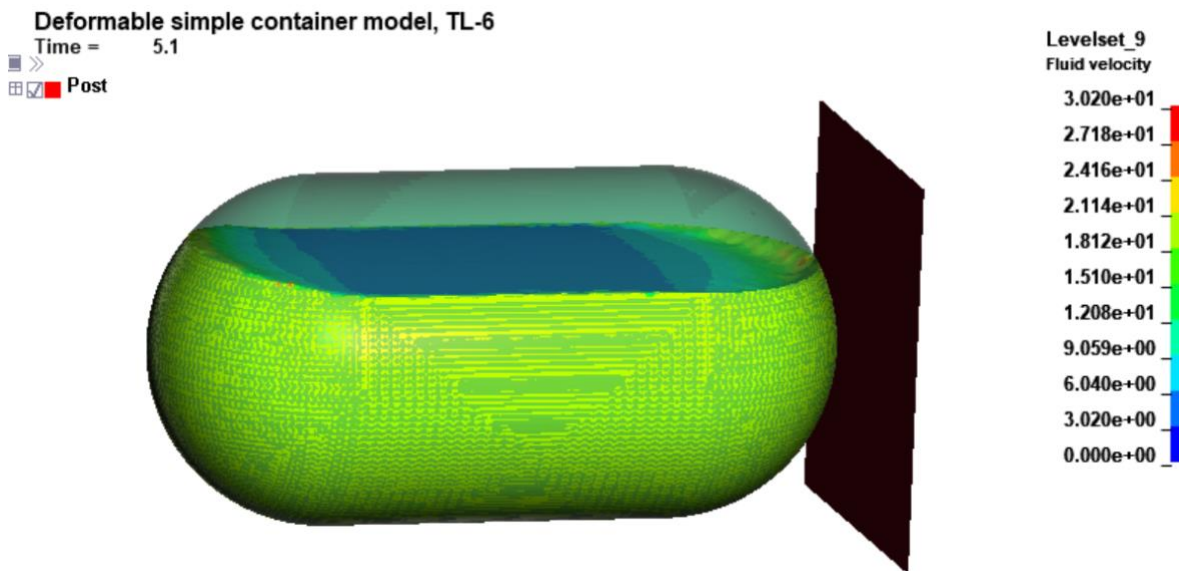


Figure 40. Sequential image of the deformable container, impacting rigid wall, $t=5.1$ ms.

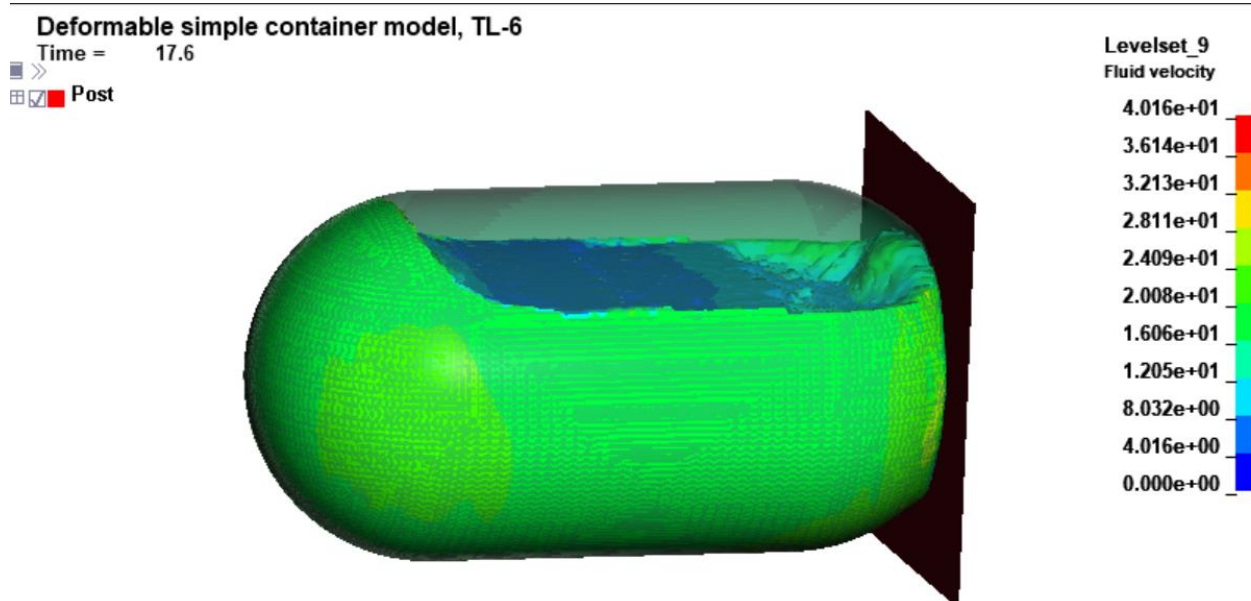


Figure 41. Sequential image of the deformable container, impacting rigid wall, $t=17.6$ ms.

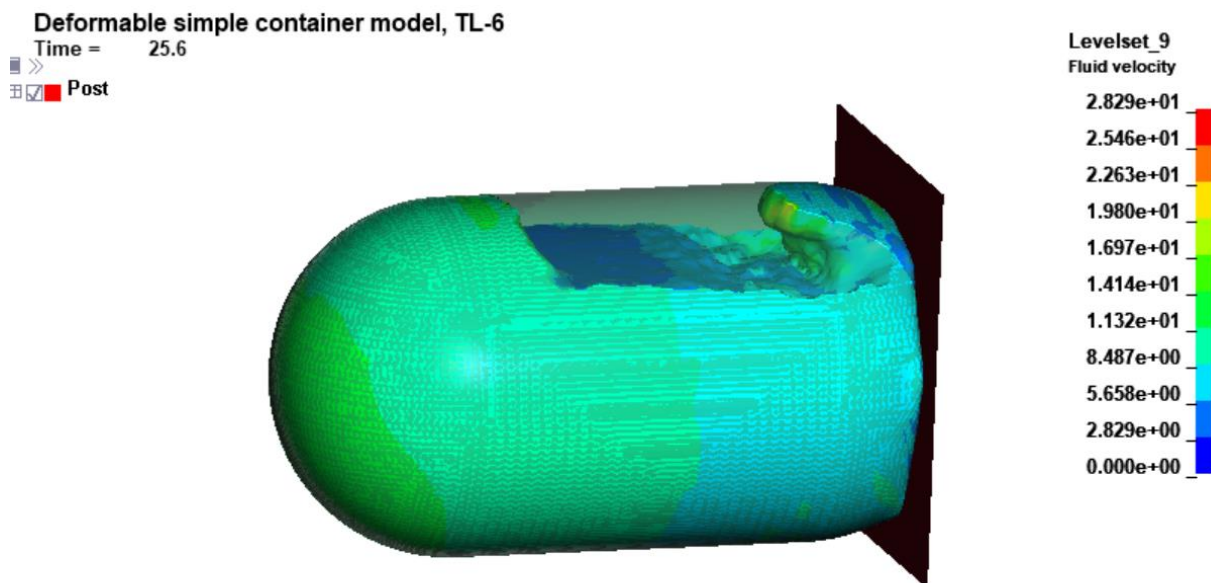


Figure 42. Sequential image of the deformable container, impacting rigid wall, $t=25.6$ ms.

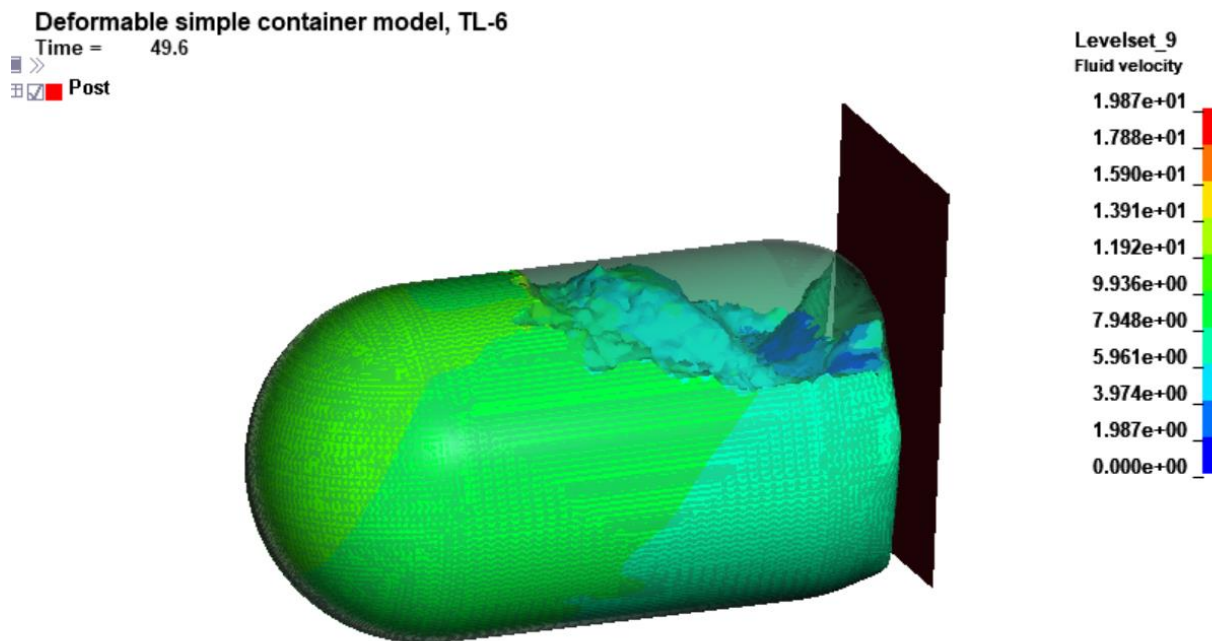


Figure 43. Sequential image of the deformable container, impacting rigid wall, $t=49.6$ ms.

From the simulation it was observed that the model was stable, there was no modeling error, there was no unstable element distortion, and fluids did not leak through the ICFD boundaries. The sloshing behavior can be further confirmed by the fluid behaviors taken on a cross-sectional plane in the middle of the container, they are shown in Figure 44 to Figure 47.

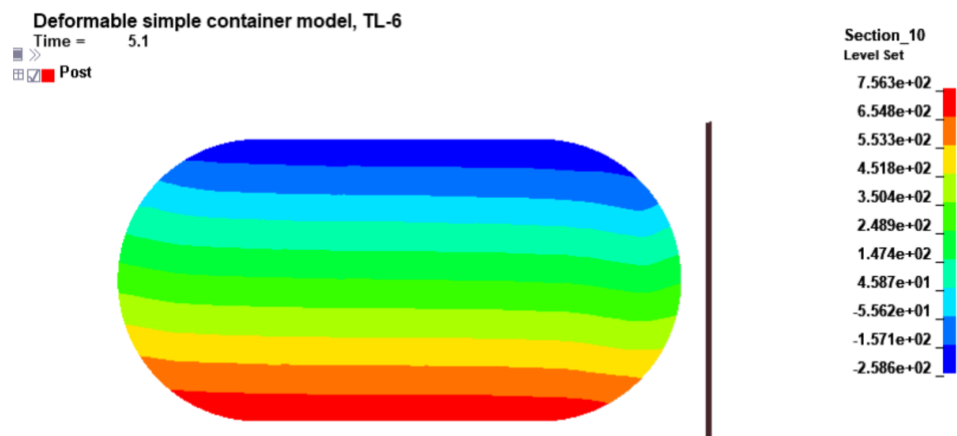


Figure 44. The sectional view of the level sets of the simulation, $t=5.1$ ms.

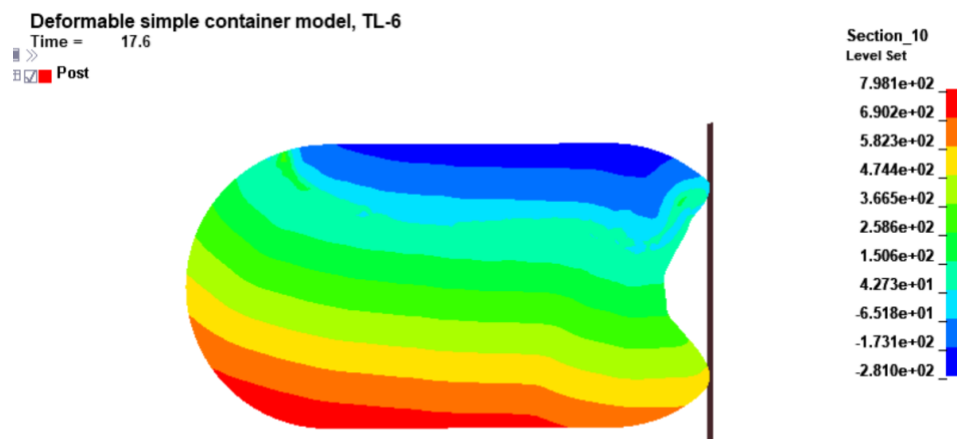


Figure 45. The sectional view of the level sets of the simulation, $t=17.6$ ms.

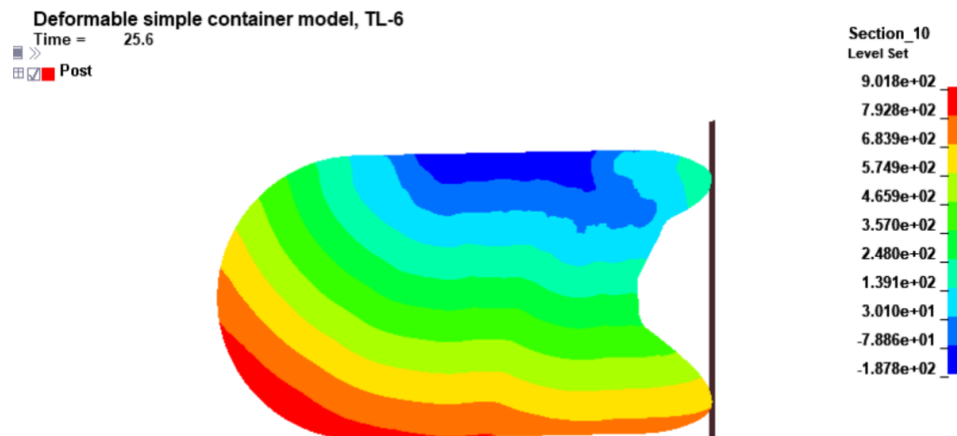


Figure 46. The sectional view of the level sets of the simulation, $t=25.6$ ms.

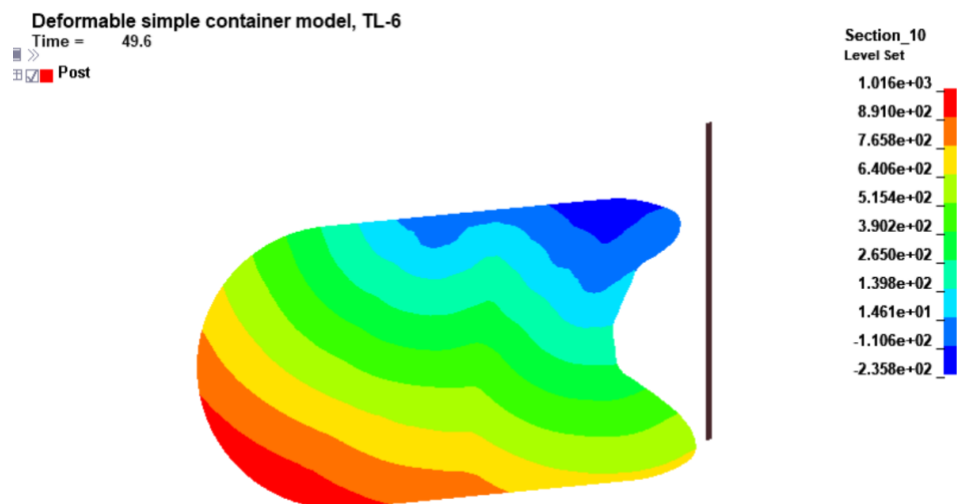


Figure 47. The sectional view of the level sets of the simulation, $t=49.6$ ms.

The impact simulation results showed that the total water volume of the container remained constant throughout the simulation, as shown in Figure 48. It was 1.072×10^9 mm³, or 1.072 m³, or 283.43 gal. of water, this value concurred with the analytically calculated water volume.

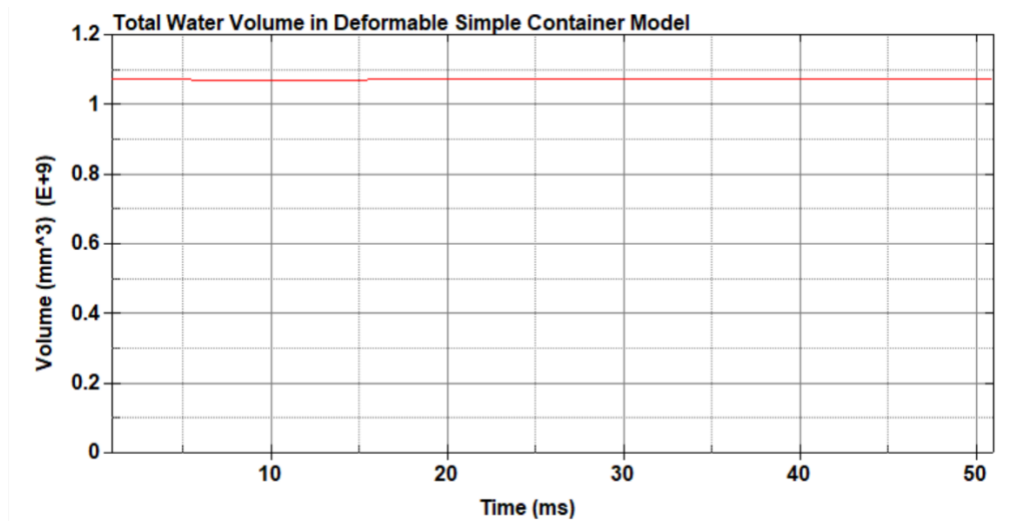


Figure 48. Fluid volume in the deformable container during impact simulation.

The simulation results show that the velocity of the container was changed from 20 m/s to -5 m/s during the simulations, as shown in Figure 49. This also confirms that the test conditions were well below one-third of the speed of sound (1500 m/s in water, gasoline etc.)

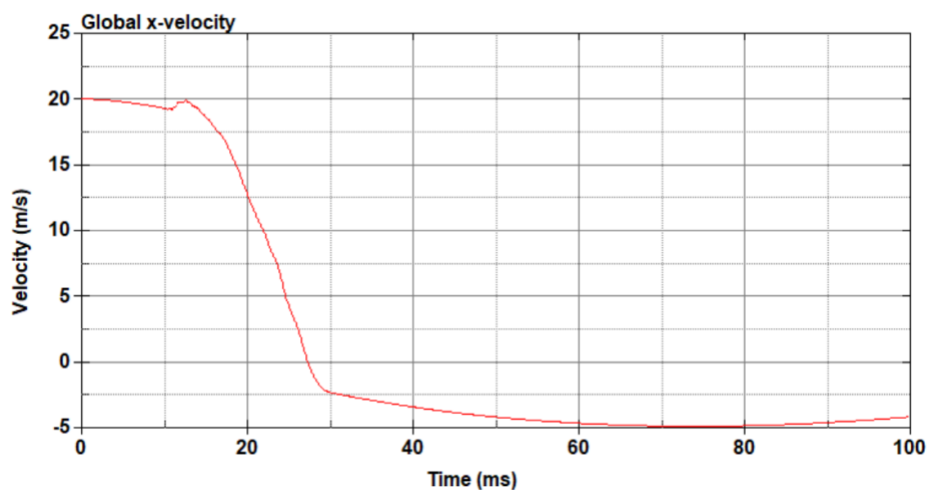


Figure 49. The change in velocity during impact simulation

4.4 Difficulties

Throughout the modeling process, various difficulties have been raised and solved accordingly. The first difficulty that was faced was the initial velocity generation problem.

There are some ways of assigning initial velocity to the system; for example, in real-world conditions, fluids in tank trailers are gradually accelerated to the vehicle's speed over potentially seconds or minutes of time. However, impact simulations often utilize hundreds of thousands of calculations within only a few seconds of time; slowly propelling the fluid to the vehicle speed similar to real vehicles this will make the model computationally very expensive and may lead to compounding long-term numerical errors.

It is preferred that models are made "ready to impact", i.e., that models have an initial velocity condition so that the state of the vehicle and fluid just prior to impact can be used in iterative simulations and relatively quickly. Assigning initial velocity to the structure results in generating a rapid change in velocity in the fluid volume, generating a pressure wave on the boundary edges like the left side edge of Figure 41. This is one of the major concerns of this model. To avoid this, the *ICFD_INITIAL card was tried. The idea was to make both the fluid volume and the structural part have the same initial velocity. Though it sounded promising, the model behaved unexpectedly. It showed an error with a message of having intersecting surfaces at a location very unrealistic.

```
*** Error 120003 (ICFD+3)
    ICFD *****
```

```
*** Error 120003 (ICFD+3)
    ICFD *****
```

```
*** Error 120003 (ICFD+3)
    ICFD *****
```

Upon consulting with other researchers, it was found that this is a prevalent issue with ICFD solvers, and the LSTC is working on improving this. It was very difficult to remove the initial wave generation, but later it was found that using the

*ICFD_CONTROL_MESH_MOV card, greatly reduced the initial wave, which can be observed in Figure 40, where, it is seen that after 5.1 ms of the simulation run time, the initial wave could not be seen.

In the future, if this becomes more problematic, it could be solved using an initial velocity applied to the objects to be impacted, for this model the rigid wall. Otherwise, the model could be allowed to settle for a small period of time before impact.

4.5 TL-6 ICFD Fluid Model Development

The main objective of this thesis was to develop a fluid model suitable for the current TL-6 vehicle model shown in Figure 1. The fluid model was developed, and it required a significant amount of time since it was a completely new approach, lacking significant previous work. In addition to these, the initial models showed very problematic behavior during development, costing the majority of the project time. However, the project is still ongoing, and researchers are working on improving the TL-6 vehicle model.

The TL-6 tanker has 4 different containers shown on Vasquez's model in Figure 1. Three of the containers have baffles in them, the function of the baffles was to prevent the fluids from having less sloshing in the longitudinal direction, as shown in Figure 50.

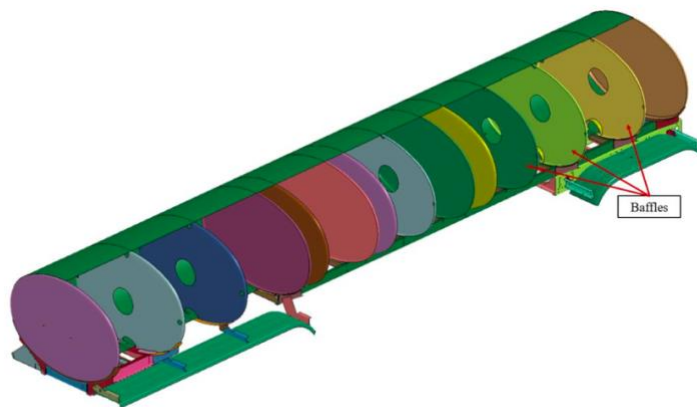


Figure 50. TL-6 tanker, container models with baffles.

However, the baffle models can be simplified to something with no orifices, i.e., a plain wall. Since the TL-6 test requires an impact at an angle of 15 degrees, most of the fluid motions are anticipated to be in the lateral direction. So, it would be potentially easier to model the baffles to a much simpler version with no orifices.

To develop the ICFD fluid model for the TL-6 vehicle, it would be best to model the smallest container of the tanker, i.e., a tanker with no baffles according to the model described in this chapter. After that, the containers with the baffles can be approached. Each baffle should be considered as a wall of the container, and different *ICFD_PART_VOL and *MESH_VOLUME cards should be defined for each of the separate fluid volumes. Care should be taken so that these fluid volumes don't have any intersecting boundary surfaces.

5 COMPARISON BETWEEN ICFD AND LAGRANGIAN MODEL

5.1 Introduction

In this chapter, a comparative study is carried out between Whitfield-Vasquez's [7] Lagrangian Fluid model and the ICFD model described in the previous chapter.

5.2 Model description

Two models were developed maintaining similar conditions, i.e. the deformable container was half filled with water, both models had the same container model, and the distance between the container and the rigid wall was the same. Both containers had an initial velocity of 20 m/s and impacted a rigid wall at an angle of 45°.

The ICFD model and the Lagrangian model assigns initial velocity to the fluid differently, that is why the initial velocity generation profile might seem discrepant to the reader. The details of this discrepancy will be discussed later in this chapter.

5.3 Simulation Results

The Lagrangian (elastic) fluid model and the ICFD model's impact simulation were performed, and many differences were observed. Figure 51 to Figure 62 shows the sequential images of the impact events.

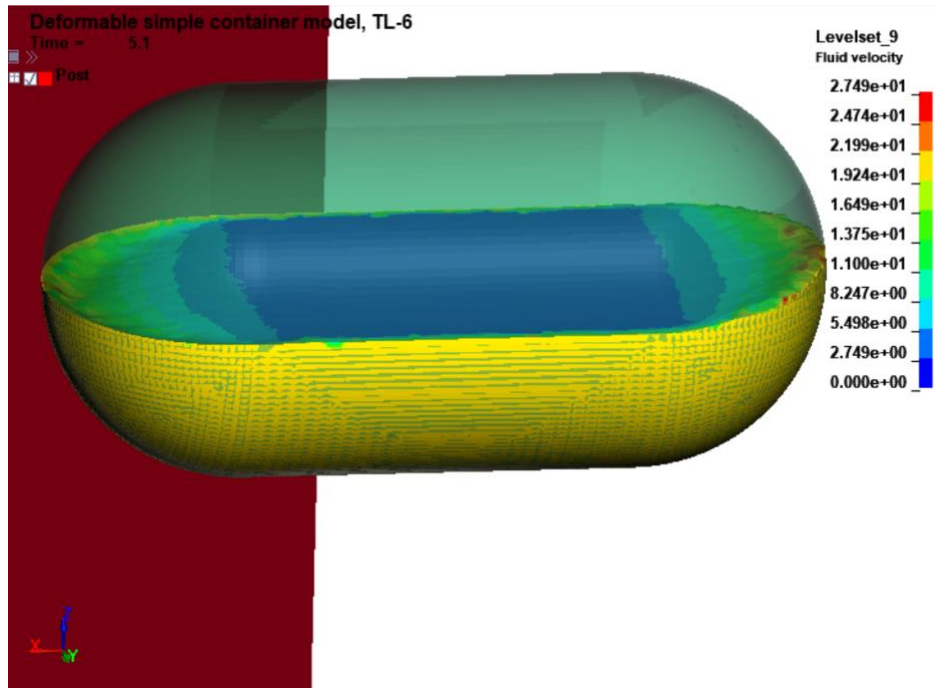


Figure 51. ICFD model simulation screenshot at impact, (t=0 ms).

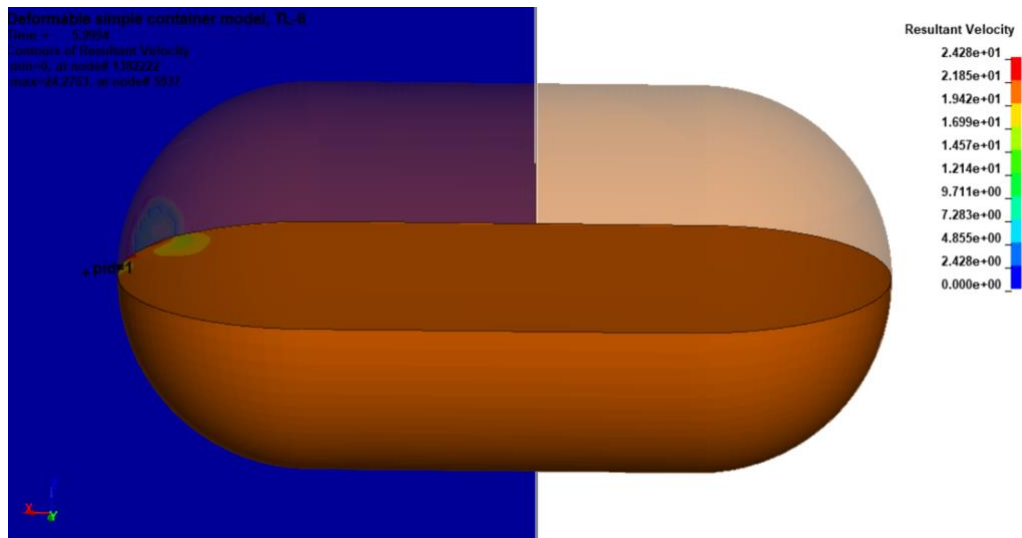


Figure 52. Elastic model simulation screenshot at impact, (t=0 ms).

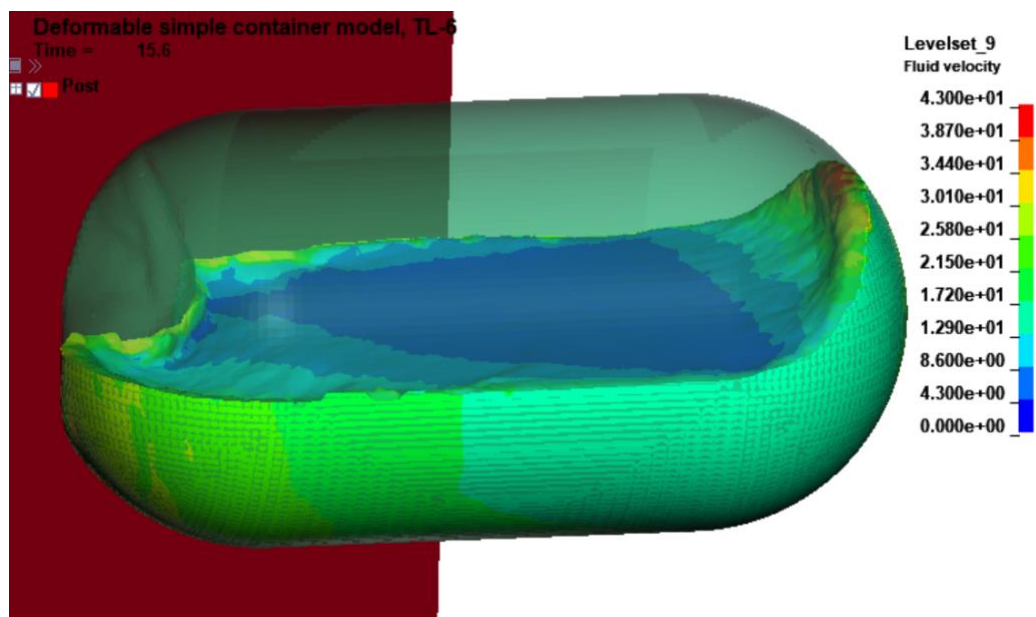


Figure 53. ICFD model simulation screenshot during impact (t=10.5 ms).

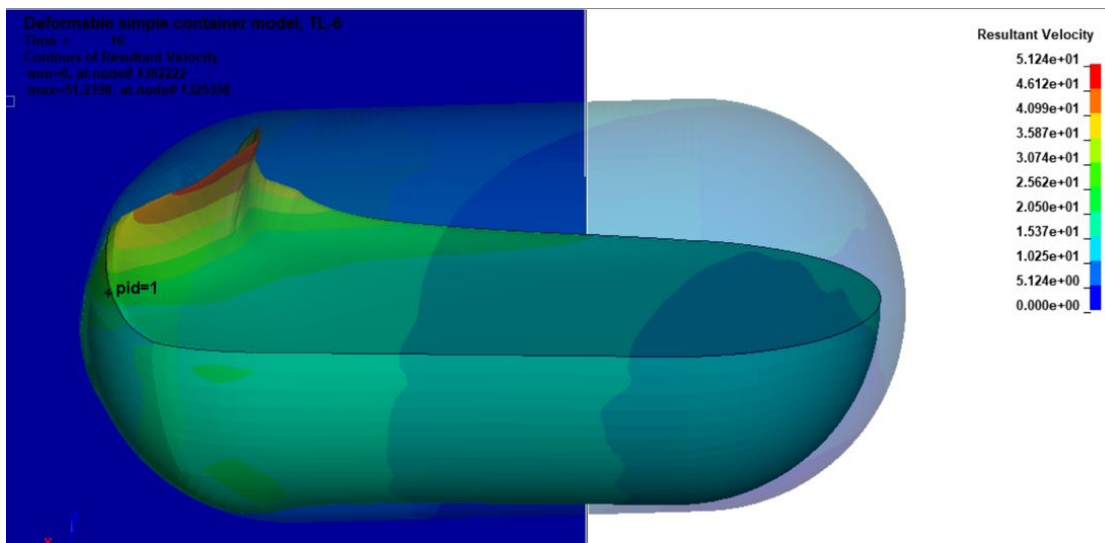


Figure 54. Elastic model simulation screenshot at impact, (t=10 ms).

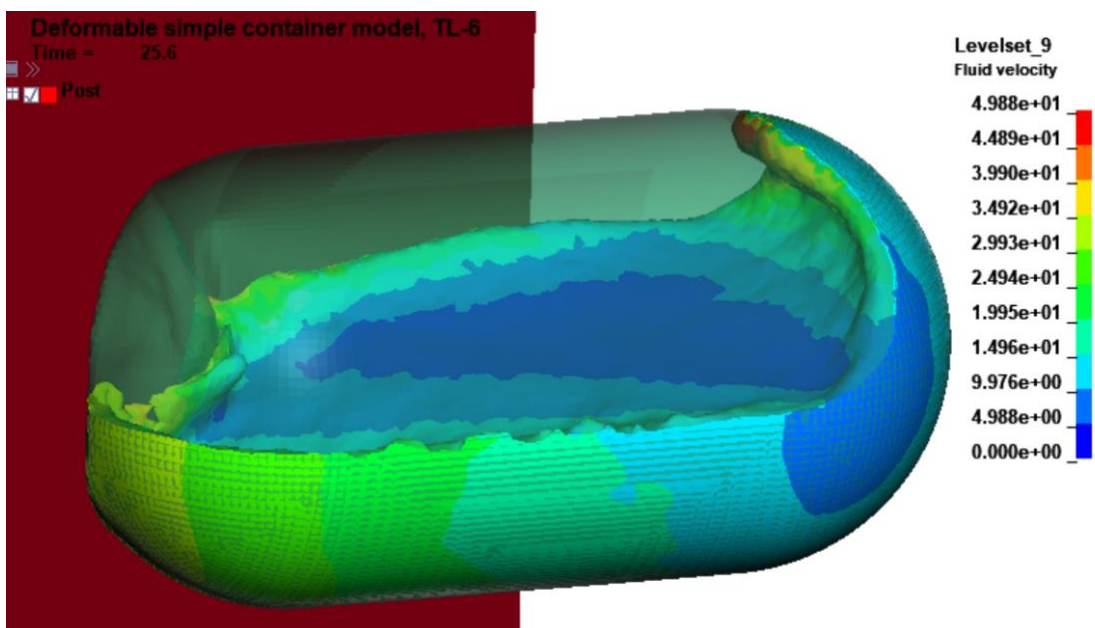


Figure 55. ICFD model simulation screenshot after impact, (t=20.5 ms).

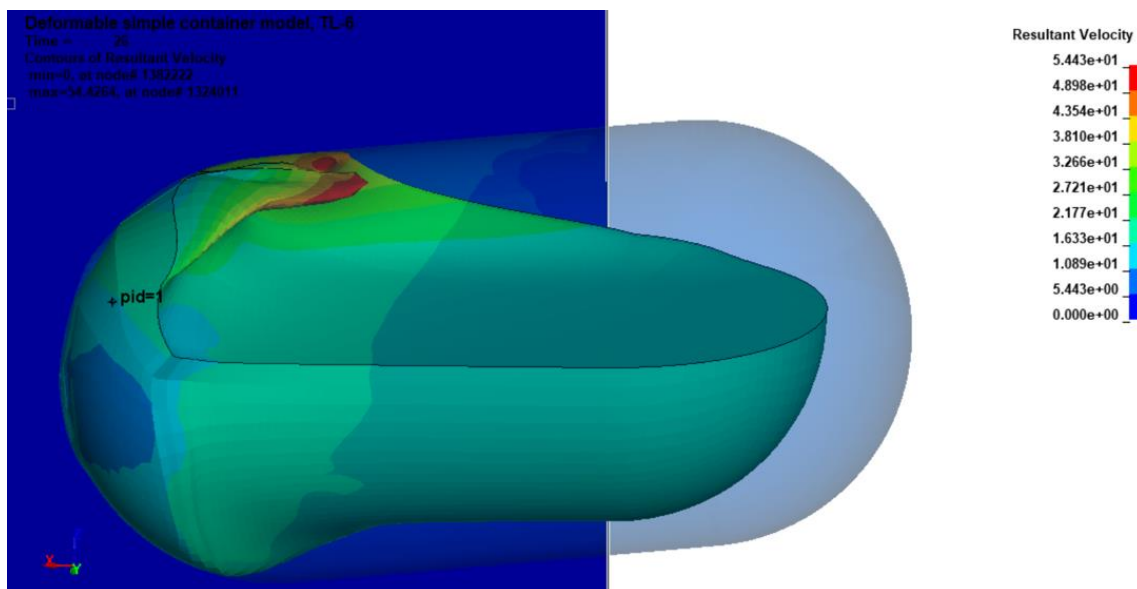


Figure 56. Elastic model simulation screenshot at impact, (t=20 ms).

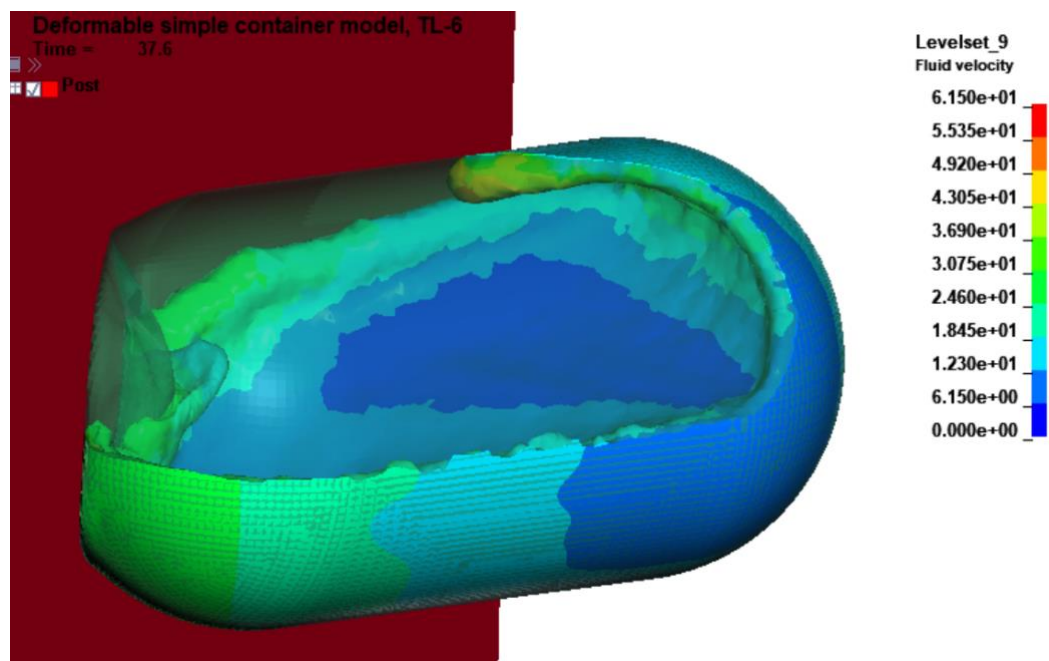


Figure 57. ICFD model simulation screenshot after impact, ($t=32.5$ ms).

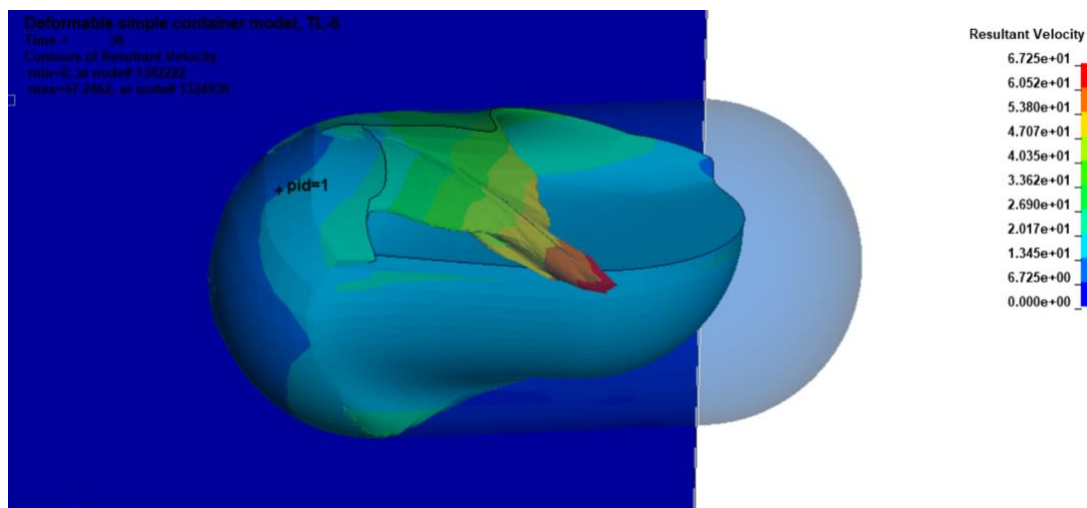


Figure 58. Elastic model simulation screenshot at impact, ($t=32$ ms).

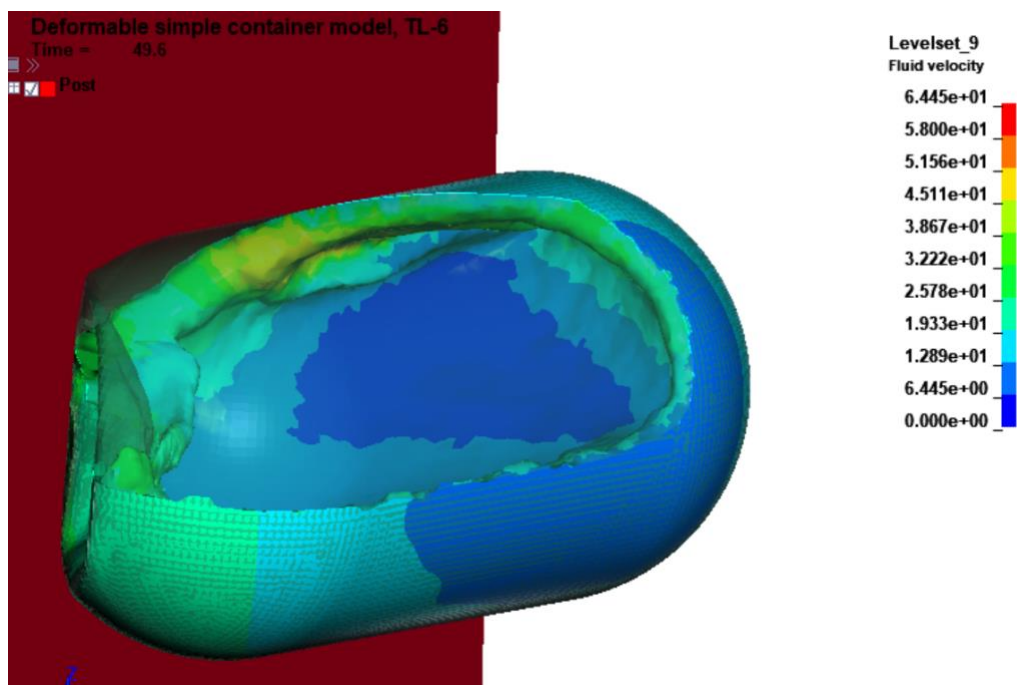


Figure 59. ICFD model simulation screenshot after impact, (t=44.5 ms).

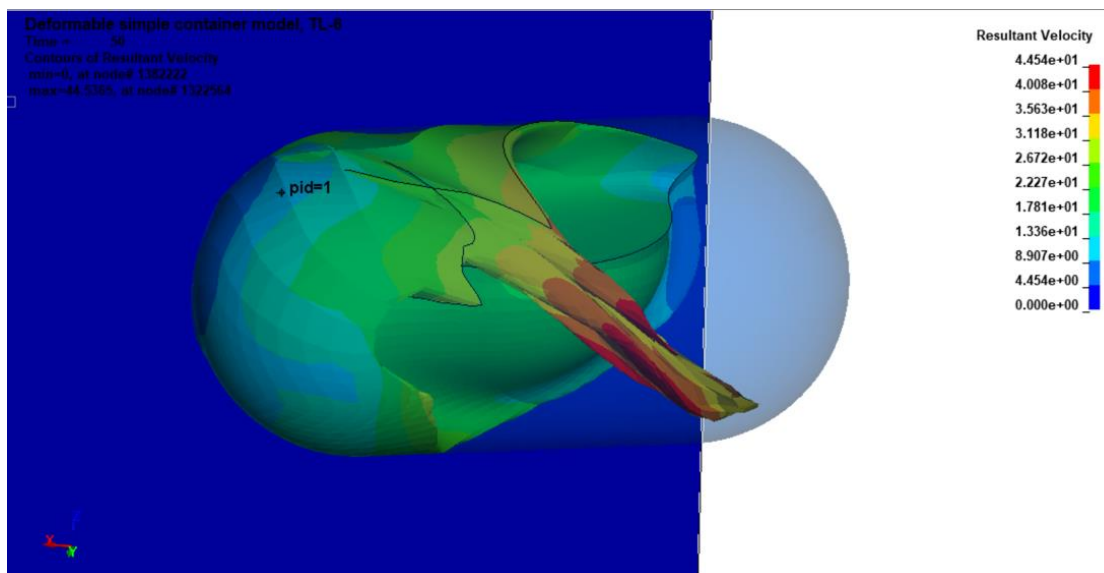


Figure 60. Elastic model simulation screenshot at impact, (t=44 ms).

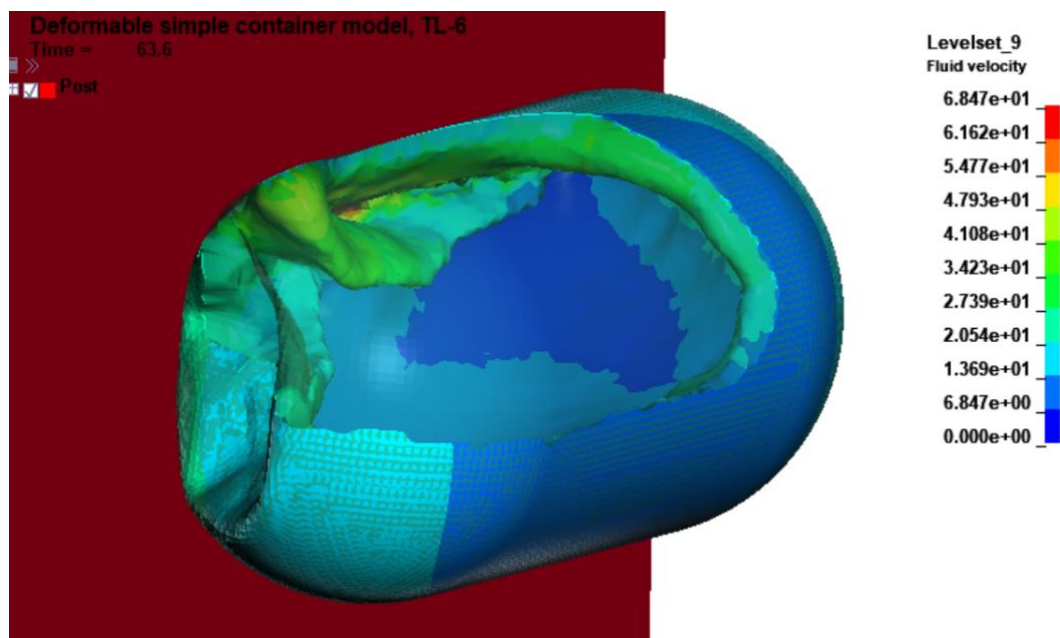


Figure 61. ICFD model simulation screenshot after impact, (t=58.5 ms).

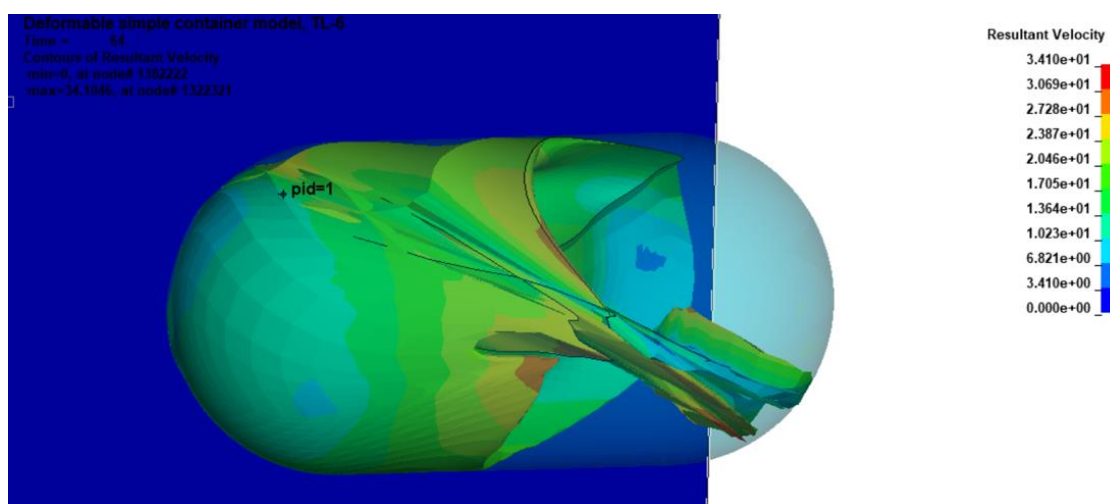


Figure 62. Elastic model simulation screenshot at impact, (t=58 ms).

From these sequential images, there are some points to be noticed. First, in ICFD the forces from the structure transfer to the fluid through every surface. That is why it is not necessary to assign an initial velocity to the fluid separately from the structure. Only one initial velocity to the fluid is sufficient. On the other hand, for the Lagrangian model,

the fluid part requires to have a separate initial velocity card. The movement of the fluid domain is not instantaneous like ICFD. Figure 63 shows a snapshot of a simulation attempt, where the initial velocity was applied to the cylinder, like ICFD. However, it can be inferred that the container's velocity was greatly reduced, and the fluid from just the right side received some of the forces, which resulted in the bulging of the fluid, as seen in Figure 63. For this reason, the initial velocity was applied to the models differently; for ICFD initial velocity was applied to the boundary layer only, whereas the Lagrangian model requires the initial velocity to be applied to the fluid domain also. Due to this, the initial wave formation of these two simulations has two different directions, as seen in Figure 53 Figure 54.

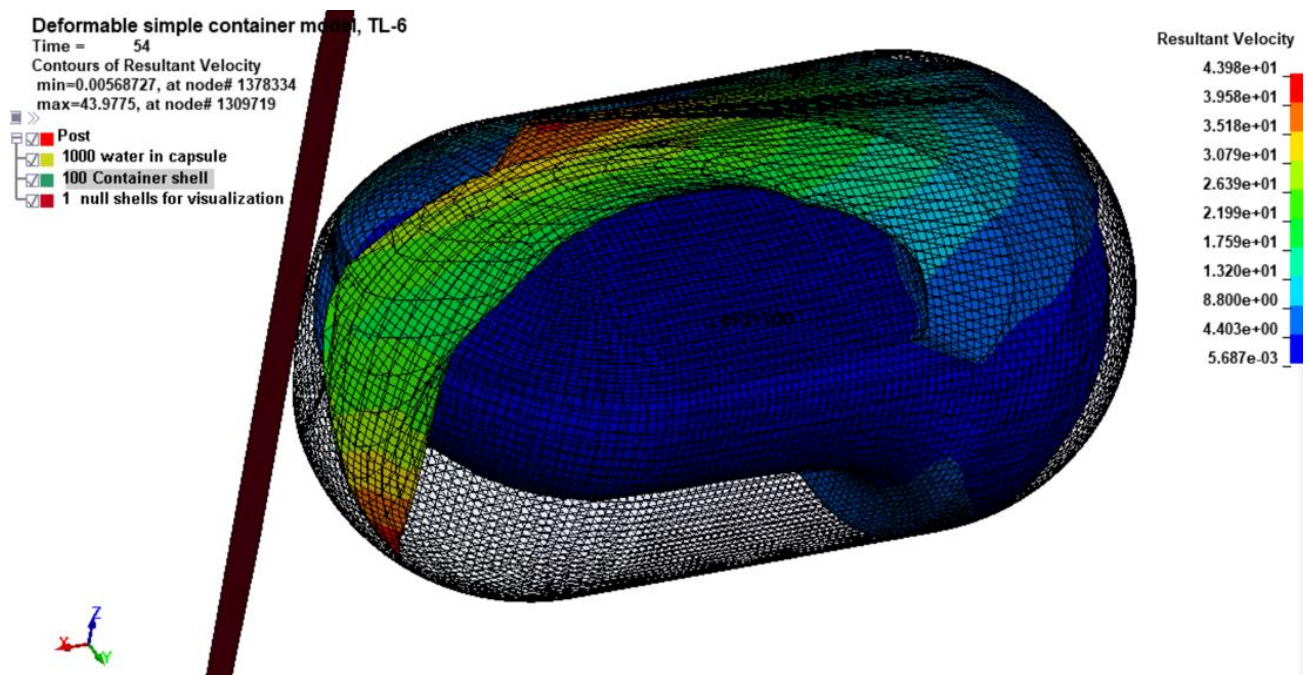


Figure 63. Initial velocity to the structure only (Lagrangian model).

From Figure 56 and Figure 58, the Lagrangian model failed to maintain the fluid boundary conditions. There is a clear separation of the fluid from the container, whereas the ICFD model maintained fluid contact throughout the impact. The Fluid elements went through a large deformation and the elements inverted creating instability.

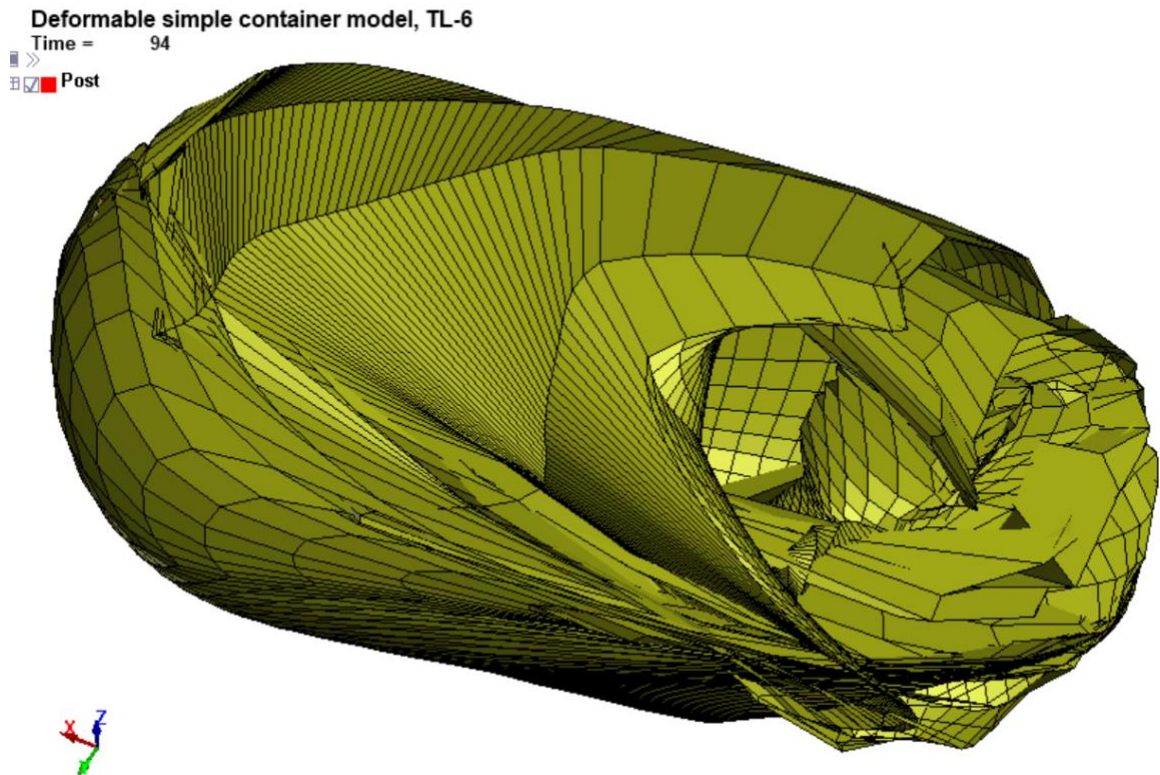


Figure 64. Element inversion in Lagrangian model.

From Figure 65, It is seen that, the global velocity in the x-direction of the container of Lagrangian model is almost linear, which doesn't portray the effect of fluid velocity in the total velocity, whereas the ICFD shows fluctuations due to the sloshing of the fluids.

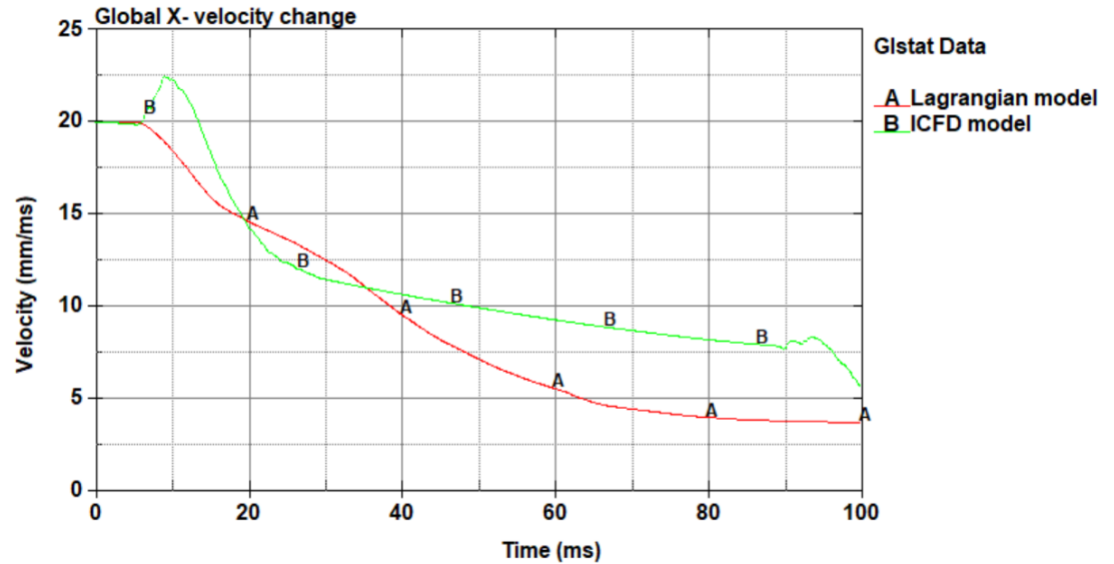


Figure 65. Global X-velocity change of the containers.

5.4 Discussion

In this chapter, the comparative study was conducted between the Lagrangian fluid model and the ICFD model. It was seen that ICFD was more stable, maintained fluid boundary conditions, and contributed to sloshing behavior. Though it is difficult to achieve the ready-to-impact model in ICFD, it shows better fluid behavior than the Lagrangian elastic model.

6 SUMMARY AND CONCLUSION

The objective of this research was to develop an ICFD model for a fluid-filled TL-6 container, which would be able to reflect the fluid sloshing behavior more accurately.

The theory and techniques behind ICFD modeling were studied. It was found that the fluid modeled is needed to be under a compressibility limit. Which is, the fluid velocity should not exceed one third of the speed of sound. A fluid to be modeled with ICFD should not exceed the speed of 500 m/s. Considering this condition it was decided that ICFD able to model the dynamic interaction of fluid and structure in the defined range.

A preliminary ICFD model was successfully developed. The model is a scaled-down version of the TL-6 vehicle model, it contained a cylindrical tank of 2m long and 1m high, containing 284 gal of water. Whereas the TL-6 vehicle contains 9,500 gallons of fluid. Future efforts will be necessary to incorporate this ICFD fluid model to the TL-6 vehicle model.

The ICFD fluid volume was generated from the surface elements, the FSI conditions were modeled, and the coupling was done to create the model. The impact of the model with a rigid wall was simulated and the simulation results were documented in this paper. The capsule shaped containers fluid motion could not be validated against any test results, due to lack of data. However, the fluid model was verified with a simpler cubic model with some validated results. With this, it can be inferred that, this fluid model can predict the behavior more accurately. The fluid sloshing behavior was achieved, and the model could be a successful way to model the fluids in the TL-6 vehicle model.

The TL-6 test used water for the ballast of the tanker containers, so, the fluid to be modeled was chosen as water. However, the tanker contains various liquids of different

properties. Mostly the fluid is gasoline, in most condition the temperature of the gasoline remains below evaporative limit, so the speed of sound in water and gasoline remains same. In those conditions also ICFD is a good choice to model. ICFD is also very useful in conditions where there is a high volume of liquids involved. The FSI models can also be used in other dynamic situations, such as, the air drag calculations of vehicles and wind turbines, modeling impacts in a submerged condition, impacts of large waves on marine structures like oil rig and different embankments, also, ICFD can be used to model sophisticated phenomena like the blood flow in the living heart.

7 FUTURE WORKS

The author could not achieve the target goal of developing the complete TL-6 vehicle model. The scale-up work could be done with the ICFD fluid model. The fluid model can be calibrated with some tests with proper documentation, and more validation with cylindrical containers before integrating the ICFD model into the TL-6 vehicle model. Since the initial model development was validated against cubic containers.

8 REFERENCES

1. NHTSA Estimates for 2022 Show Roadway Fatalities Remain Flat After Two Years of Dramatic Increases.
2. Ross, H.E., Sicking, D.L., Zimmer, R.A., and Michie, J.D., *Recommended Procedures for the Safety Performance Evaluation of Highway Features, National Cooperative Highway Research Program (NCHRP) Report 350*, Transportation Research Board, Washington, D.C., 1993.
3. *Manual for Assessing Safety Hardware (MASH)*, Second Edition, American Association of State Highway and Transportation Officials (AASHTO), Washington, D.C., 2016.
4. *Highway Accident Report – Transport Company of Texas, Tractor-semitrailer (Tank) Collision with Bridge Column and Sudden Dispersal of Anhydrous Ammonia Cargo, I-610 at Southwest Freeway*, Report Number: NTSB-HAR-77-1, National Transportation Safety Board, Washington, D.C., April 14, 1977.
5. *Highway Accident Brief, Accident Number: HWY-04-MH-012*, National Transportation Safety Board, Washington, D.C.
6. Whitfield D.L., Schmidt J.D., Faller R. K., Steelman J. S., *Investigation and Development of a Test Level 6 Barrier, Phase I*, Midwest Report No. TRP-03-404-18, Midwest Roadside Safety Facility, University of Nebraska-Lincoln, Lincoln, Nebraska, October 2018.
7. Rasmussen J.D. Stolle C.S, Faller R. K., Steelman J. S., Vasquez E., *Investigation and Development of a Test Level 6 Barrier, Phase III*, Midwest Report No. TRP-03-457-21, Midwest Roadside Safety Facility, University of Nebraska-Lincoln, Lincoln, Nebraska, October 2021.
8. ICFD theory Manual, [https://ftp.lstc.com/anonymous/outgoing/inaki/docs/pdf/icfd/ICFD theory.pdf](https://ftp.lstc.com/anonymous/outgoing/inaki/docs/pdf/icfd/ICFD%20theory.pdf).
9. Delaunay Triangulation, [https://en.wikipedia.org/wiki/Delaunay triangulation](https://en.wikipedia.org/wiki/Delaunay_triangulation).
10. Osher S. & R. P. Fedkiw. 2005. Level Set Methods and Dynamic Implicit Surfaces. Springer New York.
11. Xue, Mi-An & Zheng, Jinhai & Lin, Pengzhi. (2012). *Numerical Simulation of Sloshing Phenomena in Cubic Tank with Multiple Baffles*. Journal of Applied Mathematics. 2012, Special Issue. 10.1155/2012/245702.
12. Stolle, C.S., Vasquez, E., Fang, C., Loken, A.E., Steelman, J., Faller, R.K., Bielenberg, R.W., Rosenbaugh, S.K., Revell, J.R., and Habib, Z., *MASH TL-6 Evaluation of a 62-in. Tall, Single-Slope Concrete Median Barrier*, Midwest Report No. TRP-03-463-23, Midwest

Roadside Safety Facility, University of Nebraska-Lincoln, Lincoln, Nebraska, July 2023.

9 APPENDIX

Full ICFD model suitable for LS-DYNA is given below:

The deformable container model:

```

*KEYWORD
*PART
$#                                     title
Container shell
$#   pid      secid      mid      eosid      hgid      grav      adpopt      tmid
      100      100      100      0        0        0        0        0
*SECTION_SHELL
$#   secid      elform      shrf      nip      propt      qr/irid      icoomp      setyp
      100      2        1.0      5        1.0      0        0        1
$#   t1      t2      t3      t4      nloc      marea      idof      edgset
      3.0      3.0      3.0      3.0      0.0      0.0      0.0      0
*MAT_PIECEWISE_LINEAR_PLASTICITY
$#   mid      ro      e      pr      sigy      etan      fail      tdel
      1007.86000E-6      200.0      0.28      0.326      0.01.00000E21      0.0
$#   c      p      lcss      lcsr      vp
      40.0      5.0      0      0      1.0
$ plastic stress strain curve
$#   eps1      eps2      eps3      eps4      eps5      eps6      eps7      eps8
      0.0      0.0152      0.0226      0.0407      0.0691      0.0983      0.1345      0.7093
$#   es1      es2      es3      es4      es5      es6      es7      es8
      0.326      0.328      0.3788      0.4414      0.497      0.53      0.5557      0.7604
*INITIAL_VELOCITY_GENERATION
$#   id      styp      omega      vx      vy      vz      ivatn      icid
      100      2      0.0      20.0      0.0      0.0      0      0
$#   xc      yc      zc      nx      ny      nz      phase      irigid
      0.0      0.0      0.0      0.0      0.0      0.0      0      0
*DEFINE_CURVE
$#   lcid      sidr      sfa      sfo      offa      offo      dattyp      lcint
      700      0      1.0      1.0      0.0      0.0      0      0
$#
      a1      o1
      0.0      0.1
      1.0      0.1
      100.0      0.1
*RIGIDWALL_PLANAR_ID
$#   id                                     title
      1
$
$#   nsid      nsidex      boxid      offset      birth      death      rwksf
      0      0      0      0.0      0.01.00000E20      1.0
$#   xt      yt      zt      xh      yh      zh      fric      wvel
      1700.0      0.0      0.0      1000.0      0.0      0.0      0.0      0.0
*CONTROL_CONTACT
$#   slsfac      rwpnal      islchk      shlthk      penopt      thkchg      orien      enmass
      0.1      1.0      1      0      1      0      1      0
$
$#   usrstr      usrfrc      nsbcs      interm      xpene      ssthk      ecdt      tiedprj
      0      0      0      0      4.0      1      1      0
$#   sfric      dfrc      edc      vfc      th      th_sf      pen_sf      ptscl
      0.0      0.0      0.0      0.0      0.0      0.0      0.0      1.0
$#   ignore      frceng      skiprwg      outseg      spotstp      spotdel      spothin
      0      0      0      0      0      0      0
$#   isym      nserod      rwgaps      rwgth      rwksf      icov      swradf      ithoff
      0      0      1      0.0      1.0      0      0.0      0
$#   shldg      pstiff      ithcnt      tdcnof      ftall      unused      shltrw      igactc
      0      0      0      0      0      0.0
*CONTROL_ENERGY
$#   hgen      rwen      slnten      rylen      irgen      maten      drlen      disen
      2      2      2      1      2      1      1      1
*CONTROL_IMPLICIT_AUTO
$#   iauto      iteopt      itewin      dtmin      dtmax      dtexp      kfail      kcycle

```

```

1      100      20      0.0      -700      0.0      0      0
*CONTROL_IMPLICIT_DYNAMICS
$#  imass      gamma      beta      tdybir      tdydth      tdybur      irate      alpha
1      0.55      0.27563      0.01.00000E281.00000E28      1      0.0
*CONTROL_IMPLICIT_GENERAL
$#  imflag      dt0      imform      nsbs      igs      cnstn      form      zero_v
1      0.1      2      0      1      0      0      0
*CONTROL_IMPLICIT_SOLUTION
$#  nsolvr      ilimit      maxref      dtol      ectol      rctol      lstol      abstol
12      11      15      0.001      0.01      0.0      0.01.0000E-20
$#  dnorm      diverg      istif      nlprint      nlnorm      d3itctl      cpchk
2      1      1      3      2      10      0
$#  arcctl      arcdir      arclen      arcmtl      arcdmp      arcpsi      arcalf      arctim
0      0      0.0      1      2      0.0      0.0      0.0
$#  lsmtl      lsdir      irad      srad      awgt      sred
5      2      0.0      0.0      0.0      0.0
*CONTROL_OUTPUT
$#  npopt      neecho      nrefup      iaccop      opifs      ipnint      ikedit      iflush
1      3      0      0      0.0      0      100      5000
*CONTROL_SHELL
$#  wrpang      esort      irnxx      istupd      theory      bwc      miter      proj
20.0      1      -1      0      2      1      1      1
$#  rotascl      intgrd      lamsht      cstyp6      thshel
1.0      0      0      1      0
$#  psstupd      sidt4tu      cntco      itsflg      irqquad      w-mode      stretch      icrq
0      0      0      0      2      0.0      0.0      0
$#  nfail1      nfail4      psnfail      keepsc      delfr      drcpsid      drcprm      intperr
0      0      0      0      0      0      1.0      0
*CONTROL_TERMINATION
$#  endtim      endcyc      dtmin      endeng      endmas      nosol
100.0      0      0.0      0.01.000000E8      0
*DATABASE_GLSTAT
$#  dt      binary      lcur      ioopt
0.1      0      0      1
*DATABASE_MATSUM
$#  dt      binary      lcur      ioopt
0.1      0      0      1
*DATABASE_NODOUT
$#  dt      binary      lcur      ioopt      option1      option2
0.01      0      0      1      0.0      0
*DATABASE_RCFORC
$#  dt      binary      lcur      ioopt
0.1      0      0      1
*DATABASE_RWFORC
$#  dt      binary      lcur      ioopt
0.1      1      0      1
*DATABASE_BINARY_D3PLOT
$#  dt      lcdt      beam      npltc      psetid
2.0      0      0      0      0
*DATABASE_EXTENT_BINARY
$#  neigh      neips      maxint      strflg      sigflg      epsflg      rtlflg      engflg
0      0      3      0      2      2      2      2
$
1
$#  cmpflg      ieverp      beamip      dcomp      shge      stssz      n3thdt      ialemat
0      1      0      1      1      1      2      1

```

ICFD model keywords:

```

*ICFD_PART_TITLE
Water
$#  pid      secid      mid
1      1      1
*ICFD_PART_TITLE
Air
$#  pid      secid      mid
2      1      2
*ICFD_PART_TITLE

```

```

Interface
$#   pid   secid   mid
    3     1     1
*ICFD_PART_VOL
$#   pid   secid   mid
    10    1     1
$#   spid1 spid2   spid3   spid4   spid5   spid6   spid7   spid8
    1     3     0     0     0     0     0     0
*ICFD_PART_VOL
$#   pid   secid   mid
    20    1     2
$#   spid1 spid2   spid3   spid4   spid5   spid6   spid7   spid8
    2     3     0     0     0     0     0     0
*ICFD_SECTION
$#   sid
    1
*MESH_INTERF
$#   void
    10
$#   pid1   pid2   pid3   pid4   pid5   pid6   pid7   pid8
    3     0     0     0     0     0     0     0
*MESH_VOLUME
$#   void
    10
$#   pid1   pid2   pid3   pid4   pid5   pid6   pid7   pid8
    1     2     0     0     0     0     0     0
*ICFD_MAT
$#   mid   flg     ro     vis     st   stsflcid   ca
    1     11.00000E-61.00500E-9   0.0   0     0.0
*ICFD_MAT
$#   mid   flg     ro     vis     st   stsflcid   ca
    2     0     0.0   0.0   0.0   0     0.0
*ICFD_BOUNDARY_NONSLIP
$#   pid
    1
*ICFD_BOUNDARY_NONSLIP
$#   pid
    2
*ICFD_CONTROL_TIME
$#   ttm   dt     cfl   lcidsf   dtmin   dtmax   dtinit   tdeath
    100.0  0.0   1.0   01.00000E-91.00000E28   0.01.00000E28
*LOAD_BODY_Z
$#   lcid   sf     lciddr   xc     yc     zc     cid
    2     1.0   0     0.0   0.0   0.0   0
*DEFINE_CURVE_TITLE
Gravity force
$#   lcid   sidr   sfa     sfo     offa   offo   dattyp   lcint
    2     0     1.0   0.00981   0.0   0.0   0     0
$#
    a1     o1
    0.0    1.0
    10000.0  1.0
*ICFD_BOUNDARY_FSI
$#   pid
    1
    2
*ICFD_CONTROL_FSI
$#   owc   bt     dt     idc   lcidsf   xproj
    0     0.01.00000E28   0.25   0     0
$#   nsub
    0
*ICFD_CONTROL_MESH_MOV
$#   mmsh lim_iter   reltol
    2     100   0.001
*ICFD_DATABASE_AVERAGE
$#   dt
    5.0
*ICFD_DATABASE_DRAG
$#   pid   cpid   dtout   perout   divi   elout   ssout
    1     0     0.0     0     10     0     0

```

```
*ICFD_DATABASE_FLUX
$#      pid      dtout
      1          5.0
*END
```